Department of Construction Sciences
Solid Mechanics

ISRN LUTFD2/TFHF-5260/2024-SE(1-53)

Structural integrity analysis of a hydraulic manipulator

Master's Dissertation by

Jakob Lindborg

Supervisors:
Håkan Hallberg, Division of Solid Mechanics
Kristoffer Clasén, Fagerström industrikonsult AB

Examiner:
Jonas Engqvist, Division of Solid Mechanics

Abstract

Fagerström Industrikonsult AB has created a hydraulic manipulator equipped with a wet blasting gun for decontamination of radioactive particles from components in nuclear power plants. Verifying the structural integrity of the manipulator would enable the addition of a gripper tool, allowing manipulation of components being decontaminated, a feature requested by the industry.

The aim of this master's thesis is to verify the structural integrity of the manipulator. Load cases were identified through a dynamic analysis of a representative motion pattern. Load cases from collision scenarios were also evaluated. With the loads identified, stresses were determined using a finite element model. Stresses were analysed with respect to risk of plasticity and fatigue. Results indicate that the large aluminium sections, which constitute the majority of the manipulator, are sufficiently strong to handle the target weight. However, certain steel parts used to connect aluminium sections are at risk of plasticity, particularly in collision scenarios. The key finding is that if these steel parts are reinforced, the structural integrity of the manipulator is sufficient, allowing Fagerström to proceed with equipping the manipulator with the gripper tool.

Preface

It has been a great spring doing my masters thesis together with the Fagerström team in Helsingborg. The project has been both challenging and immensely rewarding. I want to express my gratitude to Kristoffer Clasén, my supervisor at Fagerström, for his constant support and extensive knowledge. I also want to express my gratitude to Robert Hyttfors, the "father" of the manipulator, for his detailed explanations of its workings. Additionally, I want to thank Mattias Wilborgson and Carl Johan Fagerström for their support. I have also worked closely with my supervisor at LTH, Håkan Hallberg, and I am deeply grateful for his invaluable feedback and support.

Jakob Lindborg, 21 may 2024

Nomenclature

ρ	Density	[kg/m^3]
σ	Stress	[Pa]
ν	Poisson's ratio	[-]
$R_{p0.2}$	Stress at 0.2% plastic strain	[Pa]
R_{UTS}	Ultimate Tensile Strength	[Pa]
E	Modulus of Elasticity	[Pa]
P	Pressure	[Bar]
N_i	Predicted number of loads to fatigue for specific stress range	[-]
n_i	Number of loads at specific stress range	[-]
$\Delta\sigma_c$	Reference fatigue stress range at $2 \cdot 10^6$ cycles	[Pa]
$\Delta\sigma_i$	Stress range of the maximum principal stress	[Pa]
γ_{Ff}	Safety factor regarding uncertaincies in the loads	[-]
γ_{Mf}	Safety factor regarding uncertaincies of material	[-]
m_0	Inverse slope of the fatigue strength curve in the range of 10^3 to 10^5 loads to failure	[-]
m_1	Inverse slope of the fatigue strength curve in the range 10^5 to $5 \cdot 10^6$ loads to failure	[-]
m_2	m_2 is equal to $m_1 + 2$	[-]
$\Delta\sigma_L$	Reference fatigue stress range for infinate fatigue life	[Pa]
σ_{max}	Maximum normal stress in a certain direction	[Pa]
σ_{min}	Minimum normal stress in the same direction	[Pa]
R	Defined by $\sigma_{max}/\sigma_{min}$	[-]

Abbreviations

FEM	Finite Element Method
CAD	Computer Aided Design
DOF	Degree Of Freedom

Contents

1 Introduction

1.1 Fagerström Industrikonsult AB

Fagerström Industrikonsult is a small-sized company situated in Helsingborg, Sweden. Focusing on technical solutions in various industry sectors their motto is "Designs and solutions that no one else thought of". Among notable projects Fagerström Industrikonsult are involved in is the Swedish nuclear industry, contributions to the ESS project in Lund, and participation in the Extremely Large Telescope project being built at Cerro Armazones in Chile.

1.2 Background

Fagerström Industrikonsult has developed a manipulator equipped with a wet blasting gun for the removal of radioactive particles from components used in nuclear power plants. At present, the manipulator has only been constructed as a single copy, and this unit is employed in the nuclear power plant of Forsmark.

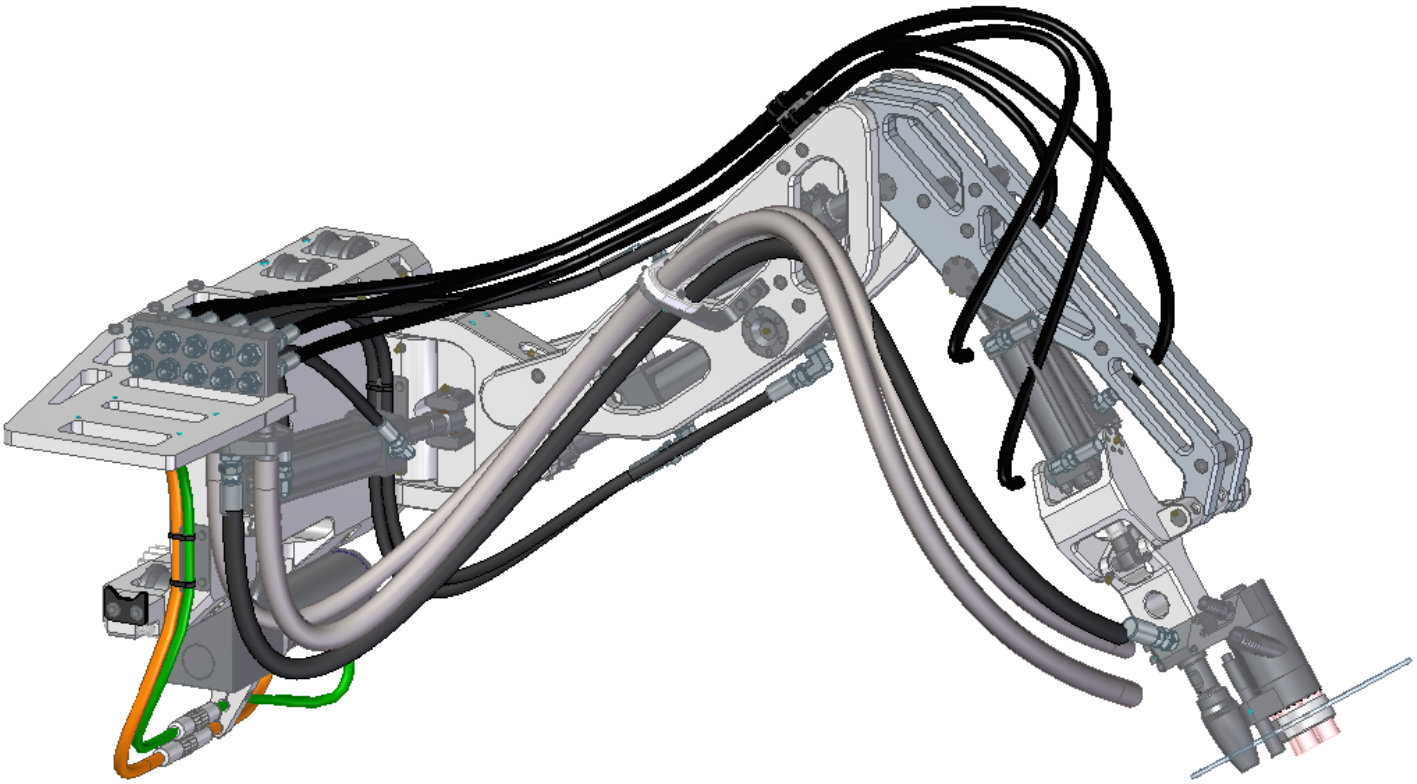

Figure 1: CAD-model of the manipulator.

Given the nature of radioactivity, the industry has shown interest to be able to maneuver the components being decontaminated without direct human involvement. Consequently, Fagerström has started to investigate the possibility of outfitting the manipulator with a gripper tool. One aspect having to be determined is the structural integrity and loading

capacity of the manipulator.

1.3 Aim and objectives

The aim of this dissertation is to validate the structural integrity of the manipulator, which will be achieved through the following objectives:

- Identify load cases. Load cases are identified through a dynamic analysis of a representative motion pattern, taking collision scenarios into consideration.
- Evaluate stresses in the sections of the manipulator for the various load cases. This is performed through FEM-analysis.
- Asses the results. Determine if the structural integrity is sufficient for lifts of the target weight. Potential structural optimizations will be evaluated.

1.4 Tools and resources

- The commercial finite element simulation software Ansys Mechanical R19.2.
- Fagerström Industrikonsult has created a CAD-model of the manipulator presented in Fig. 1, which will be used as geometry for the analysis. (Solid Edge 2022).
- 2D-drawings and data sheets associated with the various components of the manipulator.
- Eurocode 9: Design of aluminium structures [1] and Eurocode 3 – Design of steel structures [2] alongside associated documents will be used to validate the structural integrity of the manipulator. Ansys Mechanical User's Guide [3] is used to retrieve relevant theory regarding Ansys.

1.5 Limitations

- Time and computational resources limits the amount of applicable nodes/ elements.
- No input values can be retrieved from the real life manipulator.
- Only linear elastic behavior of materials is considered.

.

2 Theory

This section will provide theory about the manipulator and analysis tools. The background about the manipulator will be focused on aspects relevant for a structural analysis.

2.1 The manipulator

The manipulator is an operator-controlled robotic arm utilizing a joystick-type control. The arm contains 5 DOF, each being governed by a dedicated hydraulic cylinder. Mounted on a "linear unit", the manipulator can be moved from side to side, making it effectively a 6 DOF system when accounting for lateral movement. The high amount of DOF enables the operator to perform wet blasting from diverse angles, ensuring thorough cleaning.

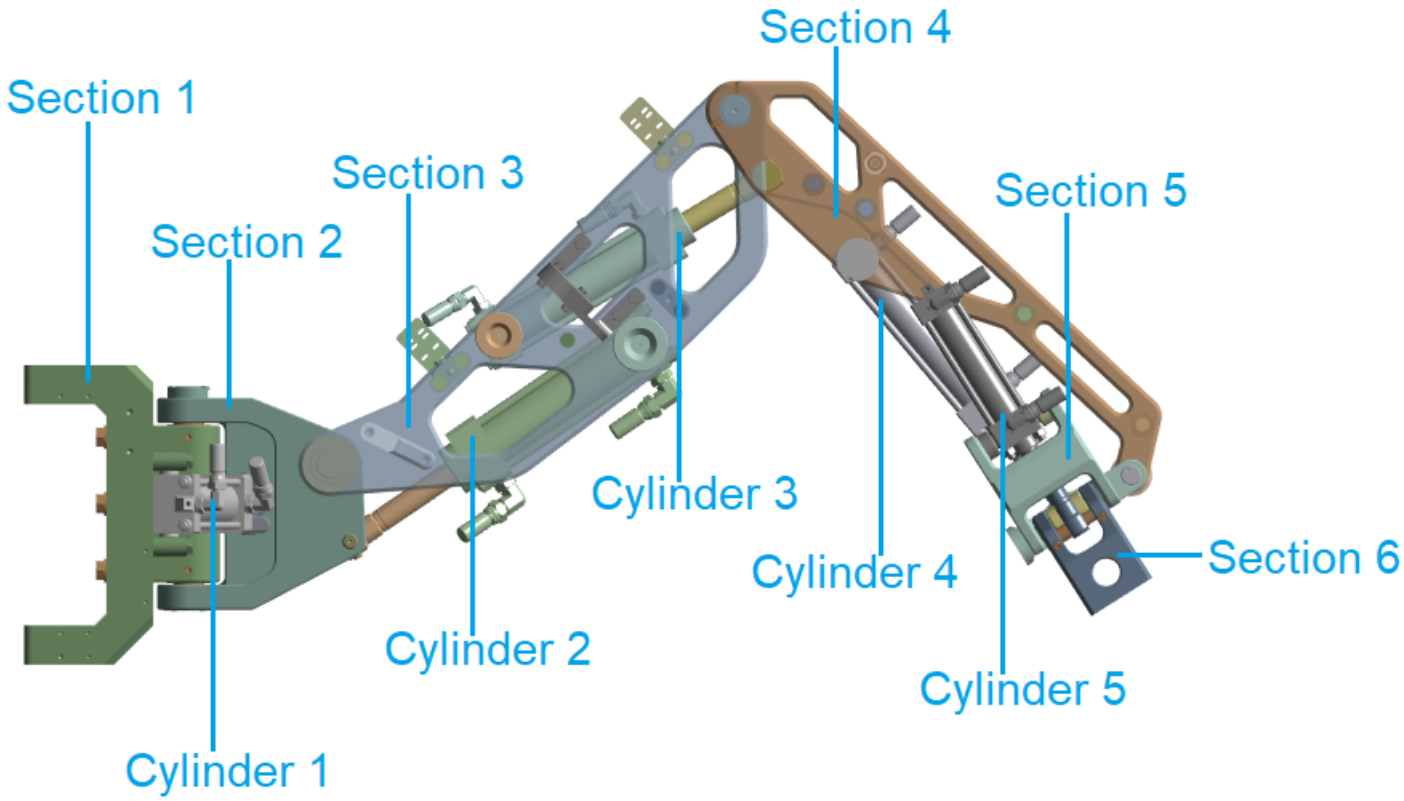

Figure 2: The various components of the manipulator.

In this report, the term "manipulator" specifically refers to the 5 DOF robotic arm displayed in Fig. 2, this figure also defines the components of interest for a structural analysis. Cylinder 1 and 5 controls horizontal movement of the wet blast tool (mounted on section 6), while cylinder 2, 3 and 4 controls vertical movement.

2.1.1 Control system

The manipulator is operated through a joystick controller, displayed in Fig. 3, which is a scaled down imitation of the manipulator, featuring a comparable 5-DOF layout. This makes handling of the manipulator intuitive for the operator. When the control system detects a difference between the orientation of the joystick controller and the manipulator, it initiates a corrective action by engaging the hydraulic cylinders in the manipulator to align it with the joysticks configuration. The system incorporates safety mechanisms triggered by two scenarios: first, if the gap in orientation becomes excessively large, and second, if the time taken to synchronize the configurations surpasses a specified limit. When triggered, the engagement of hydraulic cylinders stops.

Figure 3: The joystick controller.

2.1.2 Hydraulic system

The hydraulic cylinders are double-acting, meaning they can be engaged in both directions. The force the hydraulic cylinder can exert is greater in one direction, due to the effective areas differing on the different sides of the piston. All hydraulic cylinders in the manipulator have a similar construction as displayed in Fig. 4, however with varying diameters on the cylinder casing and piston.

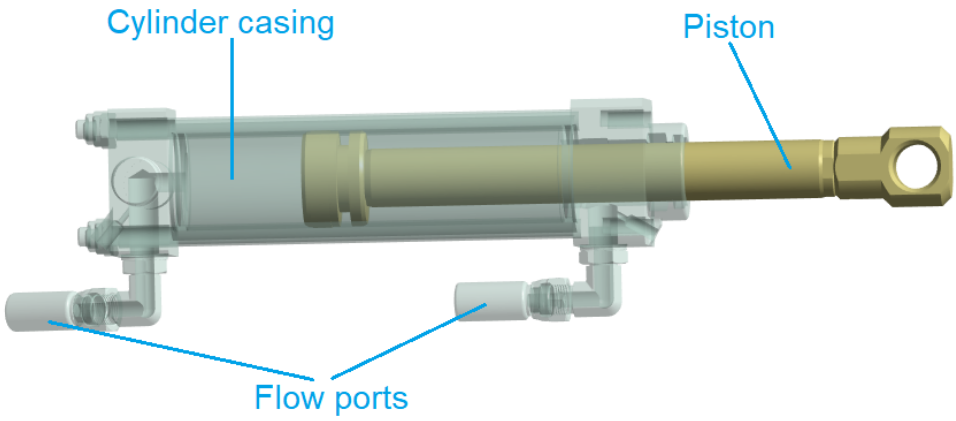

Figure 4: Double-acting hydraulic cylinder used in the manipulator.

The hydraulic cylinders are powered by a hydraulic pump, with an operating pressure that is adjustable up to 240 bars. Additionally, the hydraulic system is equipped with a pressure relief valve at 260 bars. Presently, as the manipulator is exclusively used for wet blasting, an operating pressure of around 80-90 bars is sufficient.

2.1.3 Component sourcing and in-house production

The manipulator incorporates a combination of externally sourced components and components manufactured in-house by Fagerström. The majority of the externally sourced components are irrelevant for a structural analysis. Certain sourced components however, such as the hydraulic cylinders, will be relevant for load case identification.

2.1.4 Materials and parts to be analysed

Fagerström's in-house manufactured components are made of two materials, which are the aluminium alloy EN AW-6082 T6 and stainless steel alloy EN 1.4301. Both materials have exceptional corrosion resistance, which is crucial given the manipulators exposure to high humidity due to wet blasting operations. The distribution of the materials is displayed in Fig. 5, with the material properties provided in Table 1. The analysis of the structural integrity will focus on parts manufactured by Fagerström, excluding FEM-examination of the cylinders.

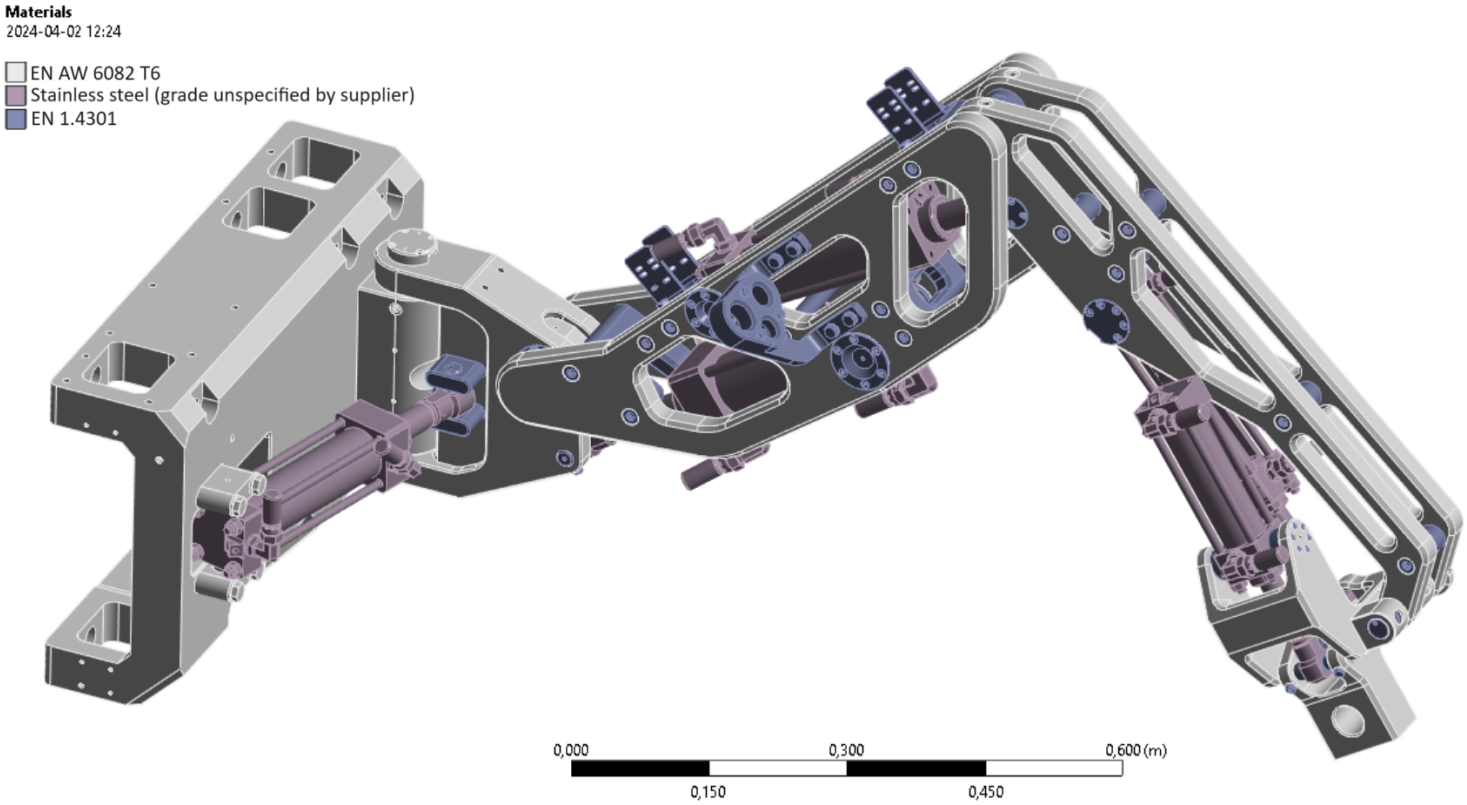

Figure 5: Material distribution of the manipulator.

Material	**EN AW 6082 T6**	**EN 1.4301**
Modulus of Elasticity [GPa]	70	200
Density [kg/m^3]	2700	7900
Poisson ratio [-]	0.3	0.3
0.2% Yield Stress $R_{p0.2}$ [MPa]	250	190
Ultimate tensile stress R_{UTS} [MPa]	290	500

Table 1: Material Properties. Aluminium properties taken from [1, p. 41]. Steel properties taken from [4, p. 7-8]

The analysis will only consider linear elastic behaviour of the materials, which assumes that the linear part of the stress-strain curve extends indefinitely. Due to this, stresses can reach levels past the R_{UTS}, which is important to keep in mind when analyzing results.

2.2 Analysis tools

Three modules of the Ansys software will be utilized for this investigation. The characteristics of them are presented here:

Ansys Rigid Dynamics: Used to analyse transient, large systems when behavior of the system can be assumed to be stiff. [3, Chapter 5.8]

Ansys Static Structural: Used to perform FEM-analysis for static cases. [3, Chapter 5.9]

Ansys Transient Structural: Used to analyse transient systems when flexibility/ deformation of bodies are of interest. Since flexibility is taken into consideration, bodies must be meshed. This module is the most computationally demanding, since bodies are meshed, and multiple time steps are analysed. [3, Chapter 5.12]

The theory on which the modules are built will be briefly described in the following section.

2.2.1 The Finite Element Method applied to 3D elasticity

After its introduction in the 1950s, FEM-analysis has become the most widely used numerical method for for solving boundary value physical problems due to its ability to solve numerical problems for an arbitrary geometry or field [5]. The method used in this report relies on FEM-analysis and therefore, it is derived in this section. The derivation of the FEM-formulation follows the method presented in [6, p.292-297]. This book presents the method for deriving 3D static elasticity, but since the method of this project includes dynamic FEM-analysis, the starting equation Eq. 1 presented in [6] is substituted with the balance of linear momentum Eq. 2 to account for dynamics. The method presented in [6] is then applied to the balance of linear momentum to derive 3D dynamic FEM-formulation.

$$\tilde{\nabla}^T \boldsymbol{\sigma} + \boldsymbol{b} = 0 \quad \text{in } \Omega \qquad \text{For static analysis} \tag{1}$$

$$\tilde{\nabla}^T \boldsymbol{\sigma} + \boldsymbol{b} = \rho \ddot{\boldsymbol{u}} \quad \text{in } \Omega \qquad \text{For dynamic analysis} \tag{2}$$

where Ω is a volume and the operator $\tilde{\nabla}^T$ is defined as:

$$\tilde{\nabla}^T = \begin{pmatrix} \frac{\partial}{\partial x} & 0 & 0 & \frac{\partial}{\partial y} & 0 & \frac{\partial}{\partial z} \\ 0 & \frac{\partial}{\partial y} & \frac{\partial}{\partial z} & \frac{\partial}{\partial x} & 0 & 0 \\ 0 & 0 & \frac{\partial}{\partial x} & 0 & \frac{\partial}{\partial y} & \frac{\partial}{\partial z} \end{pmatrix} \tag{3}$$

$\boldsymbol{\sigma}$ is the 6×1 stress tensor and $\boldsymbol{b}$ is the external body force vector (3×1 tensor). $\ddot{\boldsymbol{u}}$ is the 3×1 acceleration tensor and ρ is the density of the material. Multiplying Eq. 2 with an arbitrary weight function $\boldsymbol{v^T}$ (1×3 tensor) and integrating over Ω yields:

$$\int_\Omega \boldsymbol{v^T} \cdot (\tilde{\nabla}^T \boldsymbol{\sigma}) + \boldsymbol{v^T} \cdot \boldsymbol{b} \, \mathrm{d}\Omega = \int_\Omega \boldsymbol{v^T} \rho \ddot{\boldsymbol{u}} \, \mathrm{d}\Omega \tag{4}$$

Integrating the first term by parts and using Green-Gauss theorem yields:

$$\int_\Gamma \boldsymbol{v^T} \boldsymbol{t} \, \mathrm{d}\Gamma - \int_\Omega (\tilde{\nabla} \boldsymbol{v})^T \boldsymbol{\sigma} \, \mathrm{d}\Omega + \int_\Omega \boldsymbol{v^T} \boldsymbol{b} \, \mathrm{d}\Omega = \int_\Omega \boldsymbol{v^T} \rho \ddot{\boldsymbol{u}} \, \mathrm{d}\Omega \tag{5}$$

Where Γ denotes the boundary of Ω and $\boldsymbol{t} = \boldsymbol{\sigma n}$ denotes the traction vector on Γ. This is the weak form of 3D elasticity with dynamics. To derive the FE-formulation, several terms

will be replaced. First of all, the weight function $\boldsymbol{N}$ is used to approximate the displacement $\boldsymbol{u}$ and acceleration $\ddot{\boldsymbol{u}}$ inside elements from node values $\boldsymbol{a}$ and $\ddot{\boldsymbol{a}}$ as follows:

$$\boldsymbol{u} = \boldsymbol{N}\,\boldsymbol{a} \tag{6}$$

$$\ddot{\boldsymbol{u}} = \boldsymbol{N}\,\ddot{\boldsymbol{a}} \tag{7}$$

The weight function $\boldsymbol{v^T}$ is chosen according to Galerkin method as follows:

$$\boldsymbol{v^T} = \boldsymbol{c^T}\boldsymbol{N^T} \tag{8}$$

$\boldsymbol{c^T}$ is an arbitrary weight function. Eq. 8 together with the definition $\boldsymbol{B} = \tilde{\nabla}\boldsymbol{N}$ it follows that:

$$\tilde{\nabla}\boldsymbol{v} = \boldsymbol{B}\,\boldsymbol{c} \tag{9}$$

The constituitive relation states that:

$$\boldsymbol{\sigma} = \boldsymbol{D}\boldsymbol{\epsilon} \tag{10}$$

where $\boldsymbol{\epsilon}$ is the strain tensor. Using this relation with the kinematic relation:

$$\boldsymbol{\epsilon} = \tilde{\nabla}\boldsymbol{u} \tag{11}$$

the FEM-formulation is formulated as:

$$\int_\Omega \boldsymbol{N}^T\rho\boldsymbol{N}\,\mathrm{d}\Omega\ddot{\boldsymbol{a}} + \int_\Omega \boldsymbol{B}^T\boldsymbol{D}\boldsymbol{B}\,\mathrm{d}\Omega\boldsymbol{a} = \int_\Gamma \boldsymbol{N}^T\boldsymbol{t}\,\mathrm{d}\Gamma + \int_\Gamma \boldsymbol{N}^T\boldsymbol{b}\mathrm{d}\Gamma \tag{12}$$

Introducing the following matrices:

$$\boldsymbol{M} = \int_\Omega \boldsymbol{N}^T\rho\boldsymbol{N}\,\mathrm{d}\Omega \tag{13}$$

$$\boldsymbol{K} = \int_\Omega \boldsymbol{B}^T\boldsymbol{D}\boldsymbol{B}\,\mathrm{d}\Omega \tag{14}$$

$$\boldsymbol{f}_b = \int_\Gamma \boldsymbol{N}^T\boldsymbol{t}\,\mathrm{d}\Gamma \tag{15}$$

$$\boldsymbol{f}_l = \int_\Gamma \boldsymbol{N}^T\boldsymbol{b}\mathrm{d}\Gamma \tag{16}$$

$$\tag{17}$$

allows for the even more compact FEM-formulation:

$$\boldsymbol{M}\,\ddot{\boldsymbol{a}} + \boldsymbol{K}\,\boldsymbol{a} = \boldsymbol{f}_b + \boldsymbol{f}_l \tag{18}$$

Note 1: Often the 3D elastic dynamic FEM-formulations include a damping matrix $\boldsymbol{C}$ proportional to node velocity $\dot{\boldsymbol{u}}$. The dynamic simulations in this report did not include such damping, which is why no derivation of this term is performed.
Note 2: By removing the term $\boldsymbol{M}\,\ddot{\boldsymbol{a}}$ from Eq. 18, the 3D elastic static FEM-formulation is formulated.

2.2.2 Time integration schemes

For the Rigid Dynamics and Transient Structural analyses, a time integration scheme is required to solve the state of the system in the next time step. When it comes to time integration schemes, they can be split into two groups: implicit and explicit methods. The difference between them is that an explicit method calculates the next step solely based on the current state of the system, while a implicit method finds the next step taking both the current step and next step into consideration. The characteristics of the methods will be described in the following section, as well as how they are implemented into the modules of Ansys.

Explicit integration schemes: Explicit methods are in general computationally cheap due to their simplicity of basing the next step on the current state of the system, a drawback of this however is that explicit methods are only conditionally stable, necessitating the time steps to be small in most cases, making explicit methods most suitable for short duration transient problems [7]. The basic principle of an explicit method can be represented mathematically as follows:

$$Y_{t+1} = Y_t + f(t, Y_t)\Delta t \tag{19}$$

where t represents the initial time step, Y_t is the value of the solution at time step t, Y_{t+1} is the value of the solution at time step $t+1$, $f(t, Y_t)$ represents the update function of the system at time step t, and Δt is the time step size [8].

In the Rigid Dynamics analysis, the Runge Kutta 4 time integration was used, which falls into the category as an explicit method [3, Chapter 5.8.5.5].

Implicit integration schemes: Implicit methods are more computationally expensive, since they find the solution by using both the current and next time step, requiring solving of an algebraic equation. The upside is that implicit methods can be formulated to be unconditionally stable. This allows for larger time steps. To address the issue with computational cost, research has focused on effectively running implicit schemes on GPU units, potentially speeding up simulation time [9]. Implicit integration schemes can be described mathematically as follows [8]:

$$Y_{t+1} = Y_t + f(t, Y_{t+1})\Delta t \tag{20}$$

The specific time integration method used for the Transient Structural analysis is the HHT method, which is an implicit method.

3 Method

The overall method of the analysis is briefly presented in the following list. The procedure of each step is then presented in depth in the following sections.

1. Identify load cases. The load cases include both a normal operation of manipulator, and collisions.

    - The CAD-file is imported into Ansys. The geometry is processed for analysis. This includes removing unnecessary parts and merging small parts into components. The processing of the geometry is slightly different for the different modules in Ansys, which will be elaborated later.
    - The connections and joints are inserted into the model so that the manipulator has the same DOF as the real life manipulator. Once again, the joints are slightly different for the different modules in Ansys.
    - The dynamic movement is simulated in Ansys Rigid Dynamics, while the collsions are simulated in Transient Structural. Forces are extracted by probing the modelled joints.

2. Perform FEM-analysis of the manipulator.

    - Since there is a limit on the applicable number of nodes, the FEM analysis is ideally performed section by section to get adequate mesh quality. For the dynamic movement this strategy was employed, taking the measured forces from the Rigid Dynamic analysis and using them as boundary conditions.
    - For the collision scenario, the transformation from rigid body dynamics into a static FEM-analysis was not applicable. To capture the collision event, the dynamic simulation had to be conducted using elastic behaviour. Therefore the aluminium sections of the manipulator were meshed, and the FEM-analysis was performed directly in Transient Structural.

3. Results Evaluation. The analysis of results relies on Eurocode 9 and Eurocode 3, excluding criteria specifically tailored for construction or buildings. The standards states that an aluminium/steel structure should fulfill certain criteria, alongside providing material data for the respective materials.

3.1 Load case identification

The load cases includes both normal operation and collision scenarios. Two modules within Ansys, Rigid Dynamics and Static Structural, are employed for identifying these load cases. The manipulator's normal operation is analyzed using Rigid Dynamics, as the anticipated flexibility of components is expected to minimally impact system behavior. This choice is made due to the simplicity and low computational cost of Ansys Rigid Dynamics. The load cases analysing normal operation will be referred to as the Rigid Dynamic load cases from now on. The objective of Rigid Dynamic load case identification is to determine the forces exerted between components during moments of maximum load. These forces are subsequently utilized as boundary conditions in a FEM-analysis.
For collision scenarios, simulations will account for both flexibility of components and time, necessitating the use of Ansys Transient Structural. Since Transient Structural relies on

meshing, the stresses are retrieved directly within the module, as it was too difficult to translate the state of the system into a Static structural, section by section analysis.

3.1.1 Geometry processing

The processing of the geometry is slightly different for usage in Rigid Dynamics and Transient Structural, as Transient Structural requires some additional processing. Therefore the processing for usage in Rigid Dynamics is presented in this section, as it applies to Transient Structural. The additional processing for use in Transient Structural is then presented in its dedicated section.

The initial geometry, presented in Fig. 1 is imported into Ansys Spaceclaim (which is a CAD software included in the ANSYS software package). This geometry consists of 1200 parts ranging from solid metal sheets, tubes, hydraulic cylinders, numerous nuts and various plastic components. To simplify the geometry, parts that are not meaningful for the structural integrity (tubes, small plastic parts, seals etc) are removed. Additionally, numerous parts can be merged to further simplify the geometry. The requirements to merge parts is that they are adjacent to one another and move in unison, as well as consisting of the same material. The requirement for the merged parts to have the same material is essential for accurate material assignment and obtaining the correct manipulator weight. An example of how the merging procedure is applied to a section is demonstrated in Fig. 6. All parts are fixed to the main body. However, since the main body is made of aluminum and the rest are made of steel, section two is consolidated into five parts. Another example how the merging procedure is applied to a cylinder is presented in Fig. 7 In this case, all parts are made of steel (excluding small plastic parts, which are removed). However, the cylinder casing and piston rod must allow linear movement relative to one another, resulting in the reduction of geometries to two distinct parts.

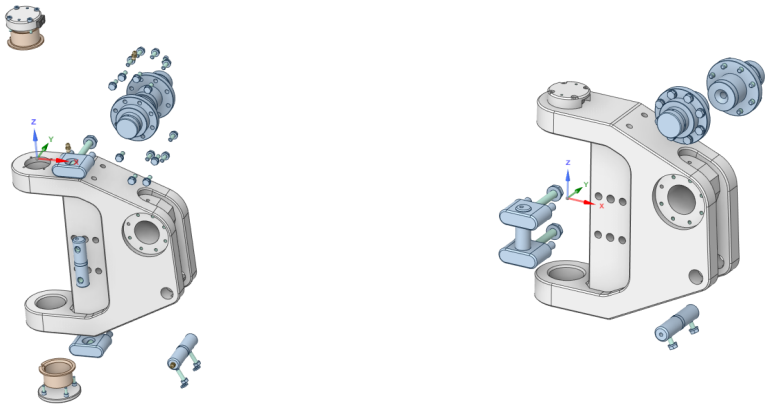

(a) Before processing (b) After processing

Figure 6: Exploded view of Section 2 before and after geometry processing. After processing, section 2 consists of 5 parts.

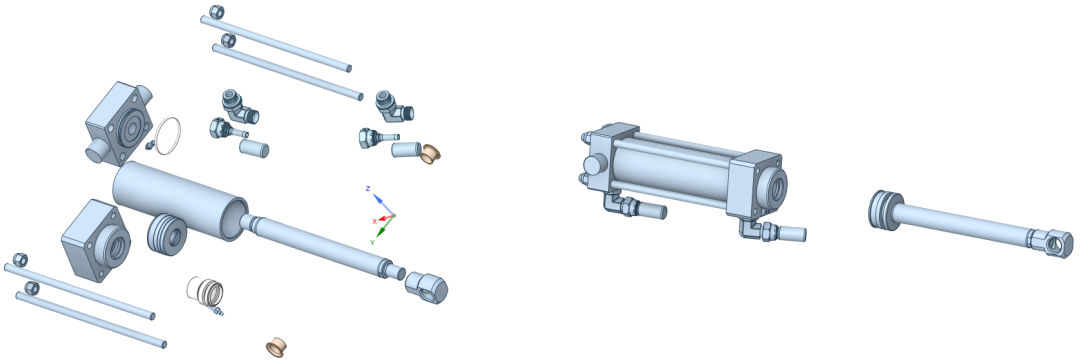

(a) Before processing (b) After processing

Figure 7: Exploded view of a cylinder before and after geometry processing. After processing, the cylinders consists of 2 parts.

After the geometry processing, the number of parts is reduced to 46. Each part is assigned its material, which is steel for all small parts and cylinders, and aluminium for the main bodies of each section. A check of the mass of the moving parts is performed (section 1 not included in weighing), which reveals that there is a slight difference in mass between the moving parts of the initial geometry, and the treated geometry. This is expected, since various tubes and small plastic parts have been removed, as well as the wet blasting tool. To account for this, the mass of the tubes and wet blasting tool are measured, and these masses are applied as point masses with similar placement as the corresponding removed part, displayed in Fig. 8. Still about 1.5kg of mass is missing, which is added to mass B as this is a central position on the manipulator.

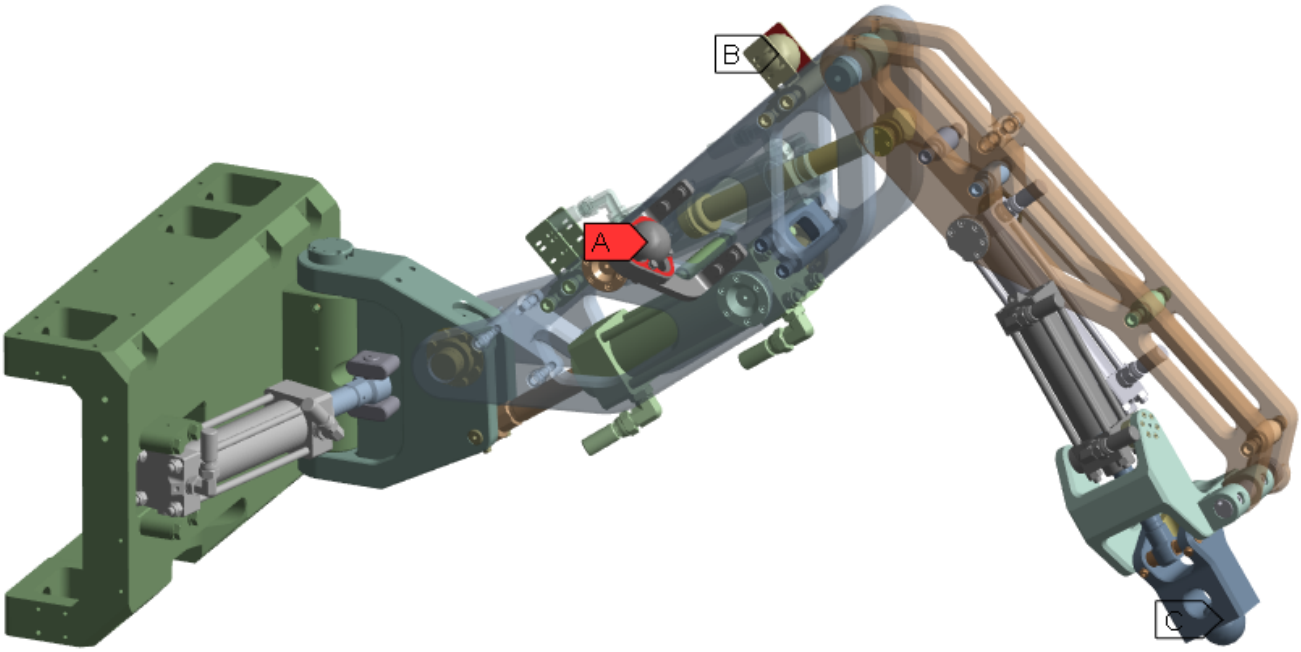

Figure 8: Manipulator after processing with point masses A, B and C to account for removed parts. The mass of the moving parts of the manipulator is 103kg.

With this geometry processing, it is prepared for the Rigid Dynamics analysis. However, for the Transient Structural analysis, further processing is necessary and this is presented in chapter 3.1.4.

3.1.2 Connections

With the geometry ready, the joints linking the components can be introduced. Once more, there are variations in how the joints are configured in Rigid Dynamics and Transient Structural. Nonetheless, the Transient Structural setup is derived from the procedure used in Rigid Dynamics, hence the Rigid Dynamics procedure is presented first. There are over 50 joints in total, so each joint is not described, instead the general procedure applying for the joints is presented.

In ANSYS, when creating a joint, two surfaces are selected to define the "reference" and the "mobile". A coordinate system appears at the center of the reference surface, and the user specifies the translations and rotations that the mobile surface can undergo relative to this coordinate system. In the case of the small parts being connected to the sections, all translations and rotations about all axes are locked, this connection type is a "fixed joint". An example of this process is presented in Fig. 9.

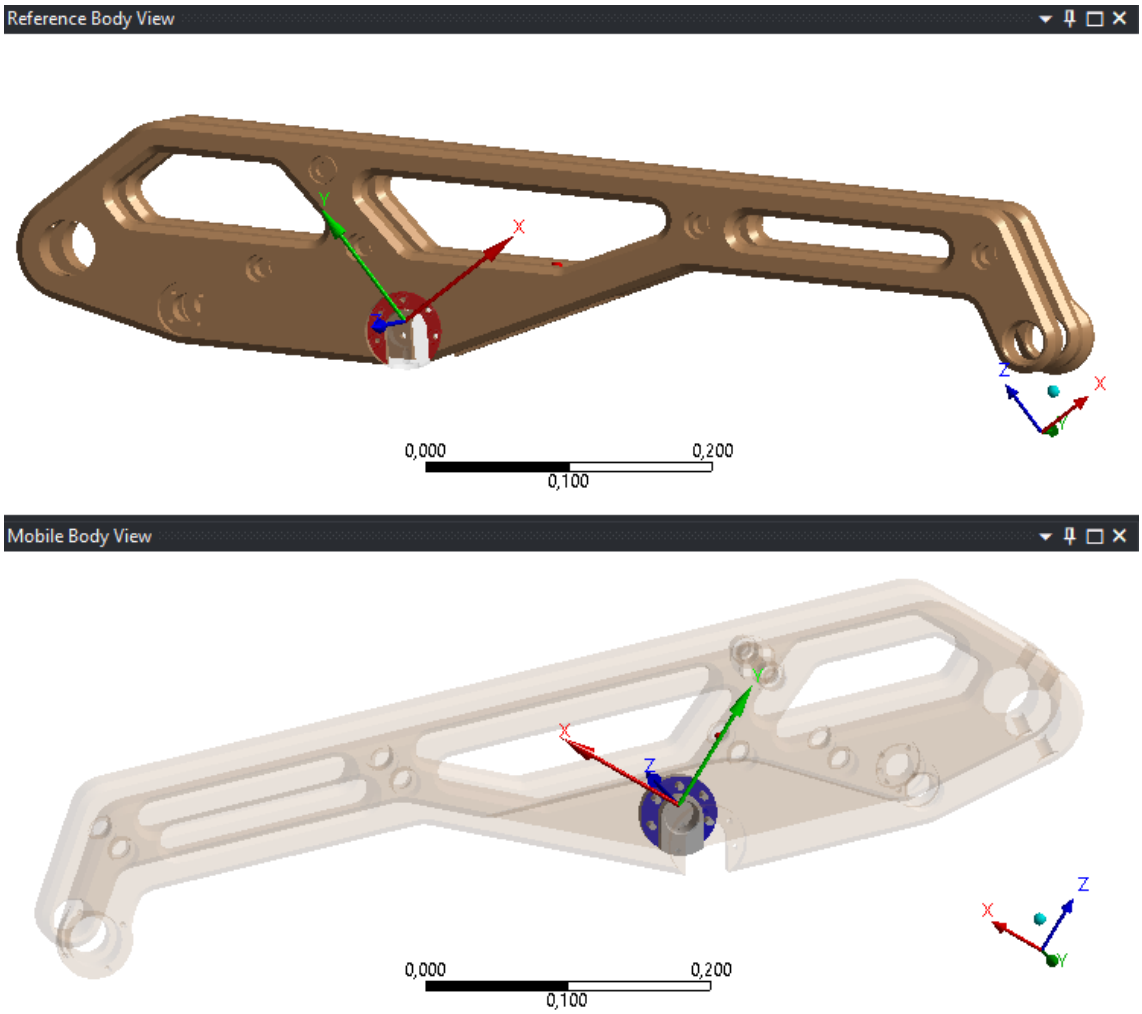

Figure 9: The referance and mobile surface used to fix a small part to section 4

Once all small parts are linked to their respective sections, the subsequent tasks involve connecting the sections to each other, enabling the manipulator to function as intended. When establishing connections between sections, it is crucial not to excessively constrain movement, as this results in non-physical load measurements in Rigid Dynamics. For instance, when connecting sections 2 and 3, as illustrated in Fig. 10, using "revolute joints" (allowing rotation about a single axis) is not feasible. This is because employing two revolute joints in parallel over-constrains the motion. Instead, two "spherical joints" (permitting rotation about all axes without translation) are utilized to appropriately distribute the load between the joints. This method of connecting two sections is used to connect all sections, since all of them are connected by two bearings in parallel.

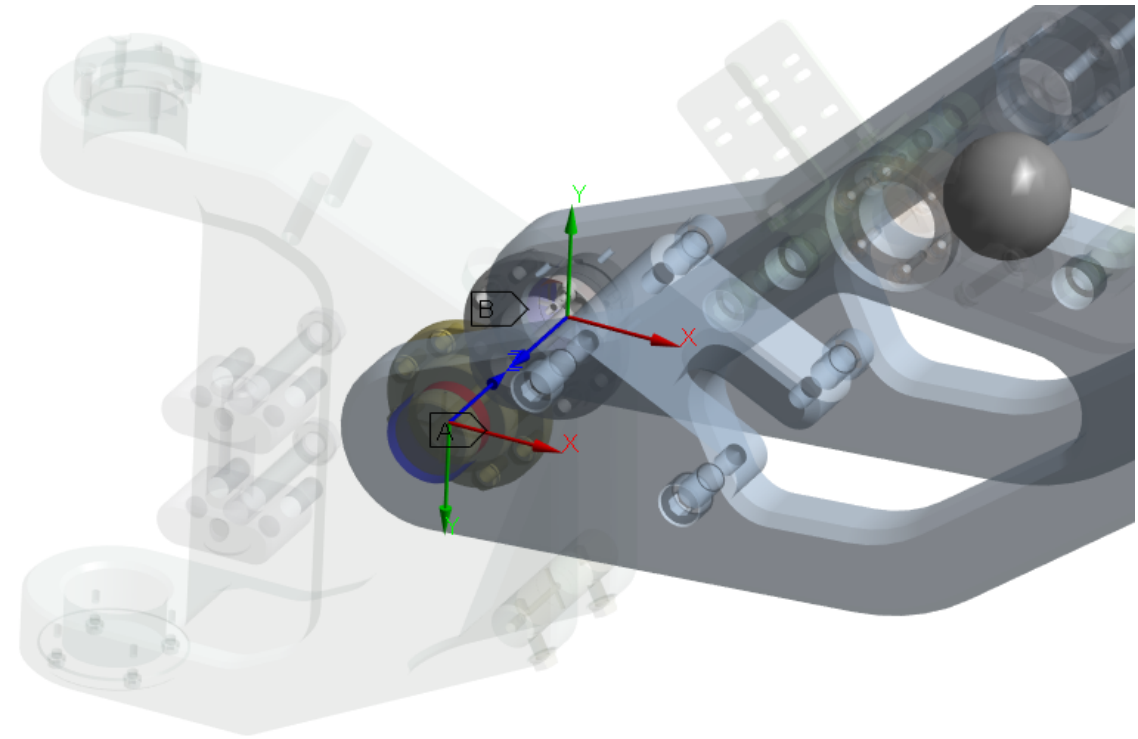

Figure 10: Two spherical joints in parallel to connect section 2 and 3.

With the sections connected, the cylinders are the remaining components to introduce joints to. The joints used in the cylinders are presented in Fig. 11. In this figure, joint A and B are spherical joints since once again, two revolute joints in paralell overconstrains. Joint D is a translational joint (allowing translation about its z axis) while joint C is a spherical joint, with the additional freedom that it can translate about its z axis. This extra degree of freedom is required to avoid over-constraining its position about the joints z axis, since it is determined by joint A and B in combination.

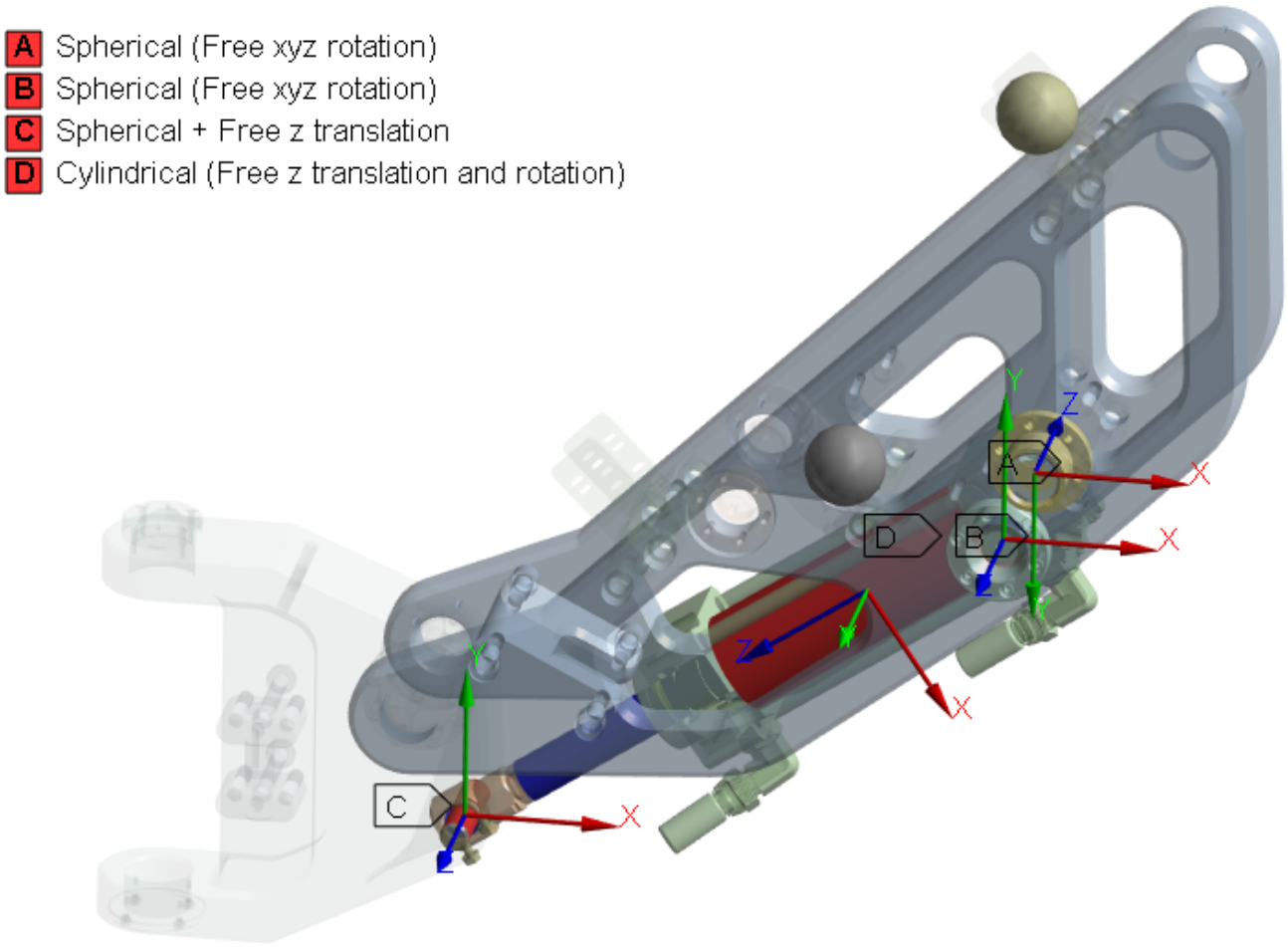

Figure 11: An example how joints are employed in the cylinders. A joints x axis is red, y axis green and z axis blue.

The methods described above can be applied to introduce all joints in the manipulator, and with all joints introduced, the model is ready to be used in Rigid Dynamics.

3.1.3 Rigid Dynamic analysis

The goal of the Rigid Dynamic analysis is to identify loads between sections during manipulation of components. This means that the manipulator is loaded with a target weight and then the various cylinders are activated so that the manipulator follows a representative motion pattern. As there is currently no gripper tool developed, it is assumed that the center of mass of the component being lifted is positioned 25 cm in front of section 6, with the component weighing 150 kg. These values were determined through discussions with Fagerström. Moreover, the loaded manipulator is assumed to move at the same speed as when unloaded, with videos provided by Fagerström for reference on maneuvering the manipulator unloaded.

To characterize the manipulator's movement, "joint loads" are applied to Joint D (displayed in Fig. 11) in cylinders 1-5. This means that the relative translational motion of the cylinder casings and pistons is what is used to define the motion of the manipulator. A simulation

time of 10 seconds with 40 time steps was selected. In each time step, the user defines the joint load for each cylinder. Ansys employs linear interpolation of joint load values between time steps, resulting in non continuities in the joint load over time. Joint loads are defined by one of the following: "relative displacement", "relative velocity", "acceleration" or "force". Initially, an attempt was made to move the manipulator using relative displacement, which did not proceed as anticipated. The discontinuities in displacement over time means instantaneous velocity changes, consequently, the measured forces between sections were non-physical. Instead, utilizing "relative velocity" was considered the most suitable approach for defining movement, as non continuities in velocity means instantaneous change of acceleration, which is physically possible. Using acceleration or force to define movement would be too cumbersome, as it is difficult to determine the precise force required to initiate or halt a cylinder's motion.

To establish a motion pattern and identify potential maximum loads, simultaneous activation of multiple cylinders was employed. Specifically, the activation of all cylinders responsible for vertical movement (cylinders 2, 3, 4) was executed simultaneously and treated as a single load case. Additionally, another load case involved activating all cylinders responsible for horizontal movement (cylinders 1, 5) simultaneously. In this scenario, the translational movement of the "linear unit" was also included, incorporating horizontal acceleration into the model to simulate this aspect. The movement of the cylinders in the Rigid Dynamic analysis can be summarised in Fig. 12. With this setup, a simulation video was established. The video was evaluated by the design team at Fagerström to ensure that the simulated motion was reasonable. After several iterations, the joint load setup was finalized, and forces excerted between sections were measured.

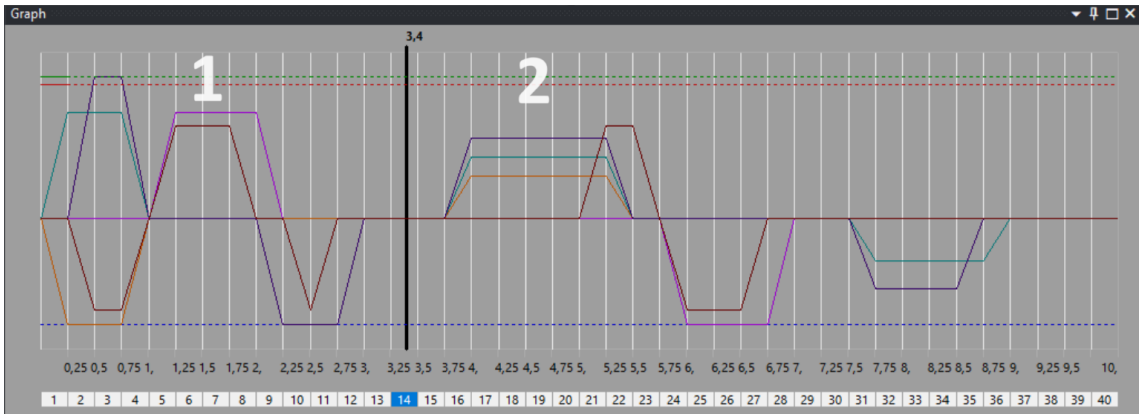

Figure 12: Velocities of cylinders during Rigid Dynamics analysis. The region marked with 1 corresponds to horizontal swing, and the region marked with 2 corresponds to vertical swing load case.

3.1.4 Collision Scenario analysis

To evaluate a collision, various methods were evaluated, and primarily two methods were considered. One was to apply an impulse on section 6, and the other was to simulate the arm colliding with a wall. A problem with applying an impulse is that it is complicated to approximate the nature of the impulse. This led to the decision to simulate the collision instead.

For the collision, the manipulator is assumed to move at the same speed upon impact as the maximum speed measured in the Rigid Dynamics analysis and to not carry a load, as the operator should exercise greater caution when the manipulator is loaded. The wall that the manipulator collides with is assumed to be completely stiff, meaning the manipulator absorbs all impact energy. Three separate collision scenarios are considered, identified as especially vulnerable positions, the difference being the direction of the swing and configuration of the arm before the impact. To accurately model the collision, flexibility of the structure must be taken into consideration, necessitating meshing. Therefore the collision can not be simulated in Rigid Dynamics and instead the Transient Structural module is used.

As mentioned previously, some extra geometry processing and alteration of joints are needed for the collision. The need for extra geometry processing arises to reduce computational cost, where some small alterations of the geometry can significantly reduce the number of elements needed to mesh a part. An example of how this is applied to a section is demonstrated in Fig. 13. All small radii, chamfers and small holes are removed from the large aluminium parts. Since only the large parts made of aluminium are meshed, the small steel parts and cylinders do not require any processing. This means that the simulation will not consider the flexibility of the small steel parts and cylinders, as they are treated as rigid.

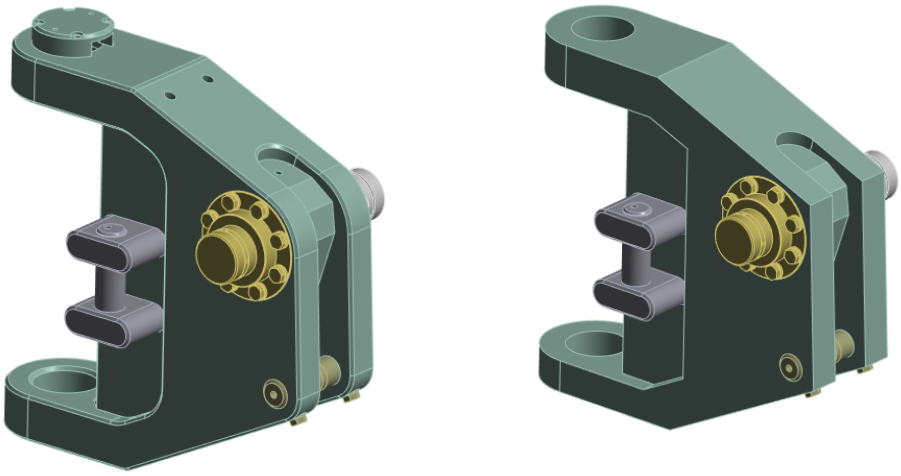

(a) Before processing (b) After processing

Figure 13: Section 2 before and after it has been treated for a collision simulation. Similar processing was made for all sections.

In addition to the geometry processing, some alteration of the joints are made, as the flexibility of the manipulator changes how the system behaves. Specifically Joint C presented in Fig. 11 is altered for all five hydraulic cylinders. No longer is the movement about the z axis free, as allowing it to translate about its z axis caused excessive translational vibration in the first collision simulation tests.

Another aspect having to be determined to model a simulation is how to set up the collision. Using "relative velocity" of the hydraulic cylinders, as used in the Rigid Dynamics analysis, to crash the manipulator into the wall is not viable, since the relative motion of the piston

and cylinder casing is unknown in the moment of impact. Additionally, as mentioned in the theory, there are two safety systems built into the system, but in the case of a collision none will activate, as neither the difference in configuration between the manipulator and joystick controller or the time limit will be reached. Therefore, it will be assumed that the hydraulic pump will increase the pressure in the hydraulic system, until the pressure relief valve of 260 bars is reached. In the first tries to simulate the collision, it was attempted to ramp up the force to corresponding to 260 bars gradually as the collision took place, but since the impact is almost instantaneous, the manipulator simply bounced off the wall with this method. With this in mind, the force was ramped up so that peak force was already reached at the moment of impact.

Collision Scenario 1

- Collision Scenario 1 evaluates a collision where the manipulator has a vertical swinging motion before impact. The manipulator is in an outstretched position prior to impact, as diplayed in Fig. 14.
- For the Collision Scenario 1, cylinder 2 is responsible for the movement of the manipulator. A joint force is used to accelerate the manipulator untill section 6 reached a speed of 1.7 m/s, as this was the highest recorded velocity of part 6 in the Rigid Dynamics simulations. Trial and error was used to identify the right amount of force. Moments before impact, the joint force exerted by cylinder 2 is increased 56 kN, corresponding to the effective area of cylinder 2 (radius of 3cm - 1.5cm piston radius) and the pressure relief valve of 260 bars.

  The other cylinders are assumed to have their flow ports closed, and with the hydraulic liquid not compressing, the only flexibility of cylinders 1 and 3-5 is assumed to come from the stiffness of the metal itself. This stiffness is represented by springs between the cylinder casing and piston.
- The wall is fixed in space and is rigid. The contact between section 6 and the wall is frictionless.
- A simulation time of 0.5 seconds was used. The temporal resolution is 100 steps per second before the impact, and 10 000 steps per second in the moments before and after impact.

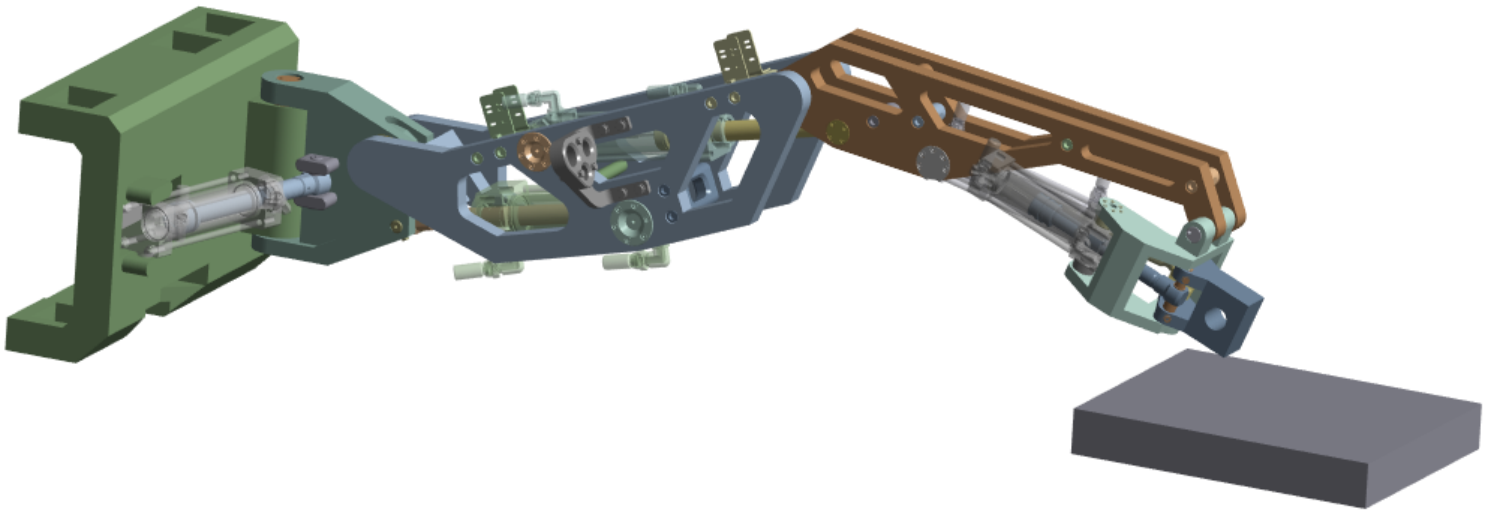

Figure 14: Setup of the manipulator and wall for Collision Scenario 1.

Collision Scenario 2

- Collision Scenario 2 evaluates a collision with an outstretched position of the manipulator, where the manipulator performs a horizontal swinging motion prior to impact, as displayed in Fig. 15.
- The same procedure as in Collision Scenario 1 is used for the acceleration of the manipulator, but to get a horizontal movement cylinder 1 is activated instead. The joint force exerted by cylinder 1 is increased 51kN moments before impact, corresponding to the radius of 2.5cm of cylinder 1 and the pressure relief valve of 260 bars. The stiffness of the other cylinders are just like in Collision Scenario 1 represented by springs.
- The same simulation time settings and fixing of wall as in Collision Scenario 1 is used.

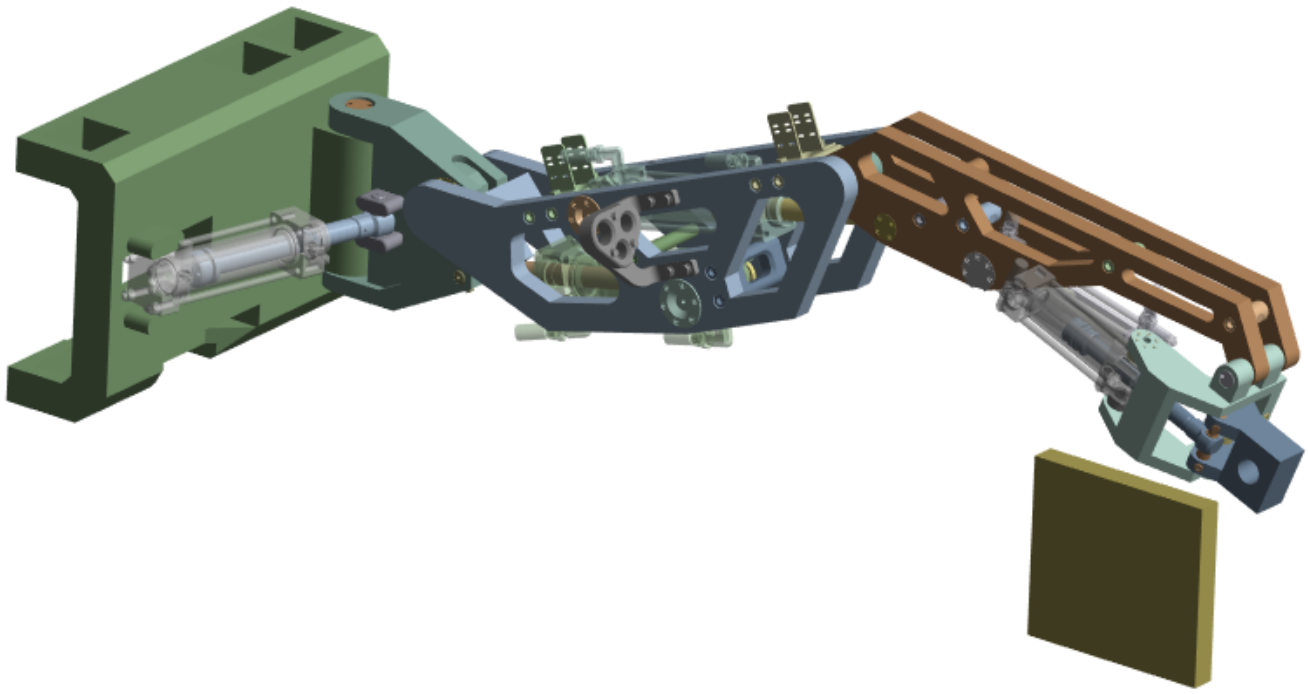

Figure 15: Setup of the manipulator and wall for Collision Scenario 2.

Collision Scenario 3

- Collision Scenario 3 also evaluates the manipulator colliding with the wall with a horizontal swinging motion at the moment of impact, just like Collision Scenario 2. The difference being the configuration of the manipulator at the moment of impact. In Collision Scenario 3 the manipulator is in a curled up position, as this position causes a "twisting" effect, especially in the region connecting section 3 and 4. The configuration of the manipulator is displayed in Fig. 16.
- The same procedure as in Collision Scenario 2 is utilized to accelerate the manipulator, with a joint force applied to cylinder 1 to accelerate the manipulator. Moments before impact, the joint force is increased to 51kn.
- The simulation time, time step, contact settings and fixing of the wall are the same as in Collision Scenario 1.

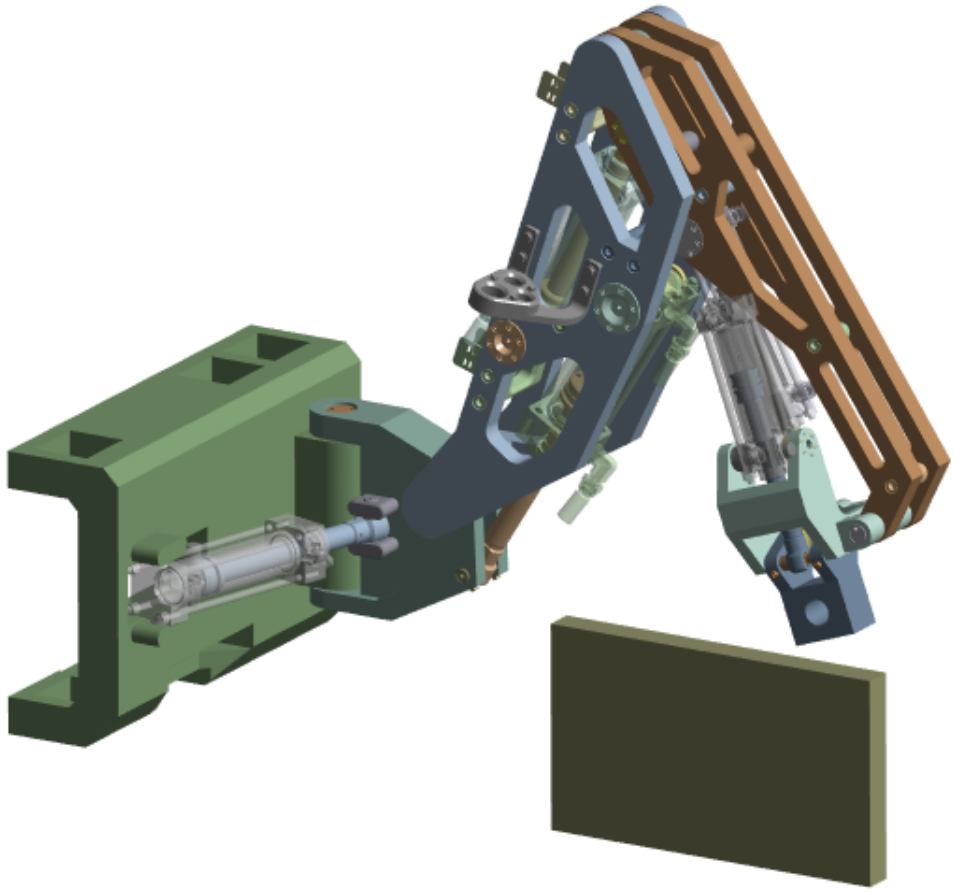

Figure 16: Setup of the manipulator and wall for Collision Scenario 3.

3.2 FEM-analysis of the manipulator

For computational efficiency, the FEM-analysis is ideally made section by section to get a mesh of higher quality. To do this, the state of the system needs to be translated from the load case identification to an individual section. Originally, the idea was to use this approach for both the Rigid Dynamics analysis and Collision Scenarios, however, during the simulations of collisions the geometry experienced substantial non-rigid behaviour which made it impossible to translate the transient structural analysis into a static structural analysis. Therefore, the FEM-analysis is made in two different ways, with the FEM-analysis method for the Rigid Dynamics analysis presented firstly.

3.2.1 FEM-analysis of Rigid Dynamics load cases

In Static Structural, the geometry must be fixed in space to avoid rigid body motion. This leads to the first step in the FEM-analysis, which is to fix the section to the ground. An example of how a section is fixed is demonstrated in Fig. 17 where the joints fixing section 3 to ground are demonstrated. Even though the cylinders are not analyzed, they are still necessary to include, since the response force in joint A and B is parallel to the cylinder, which is possible to replicate with this setup. The angle between the section and cylinder must be the same in the FEM-analysis and moment of the Rigid Dynamics analysis being evaluated.

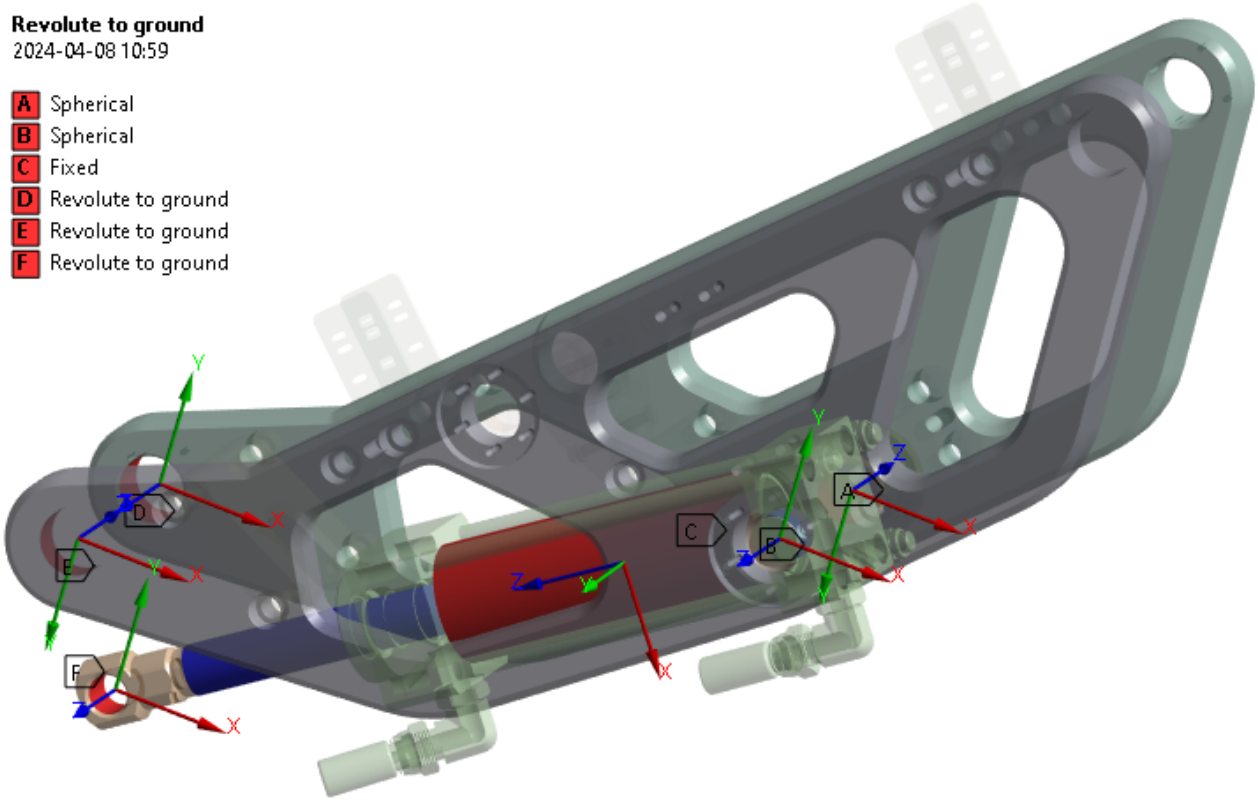

Figure 17: Joint setup of section 3 for the FEM-analysis.

The forces and loads applied are illustrated in Fig. 18. The forces B-E are determined at the moment of maximum load in the Rigid Dynamics analysis and then applied to the

FEM-analysis. Besides these forces, body loads are included to consider the acceleration of the system. This step is crucial for accurately transferring the system's state into the FEM-analysis of the sections. The procedure for obtaining and applying these accelerations is as follows: Consider viewpoint F as the "origin". In the Rigid Dynamics analysis, measure the acceleration of point F (a_x, a_y, a_z) in the global coordinate system. Additionally, measure the angular acceleration of the section about point F $(\alpha_x, \alpha_y, \alpha_z)$ (coordinate system fixed to point F). Both these measurements are also taken at the moment of maximum load of the system. With these forces and loads applied, the state of the system should be fully translated into the FEM analysis, which can be verified by comparing the response force vector in joint (D-F) in Fig. 17 to the corresponding force vector in the Rigid Dynamics analysis.

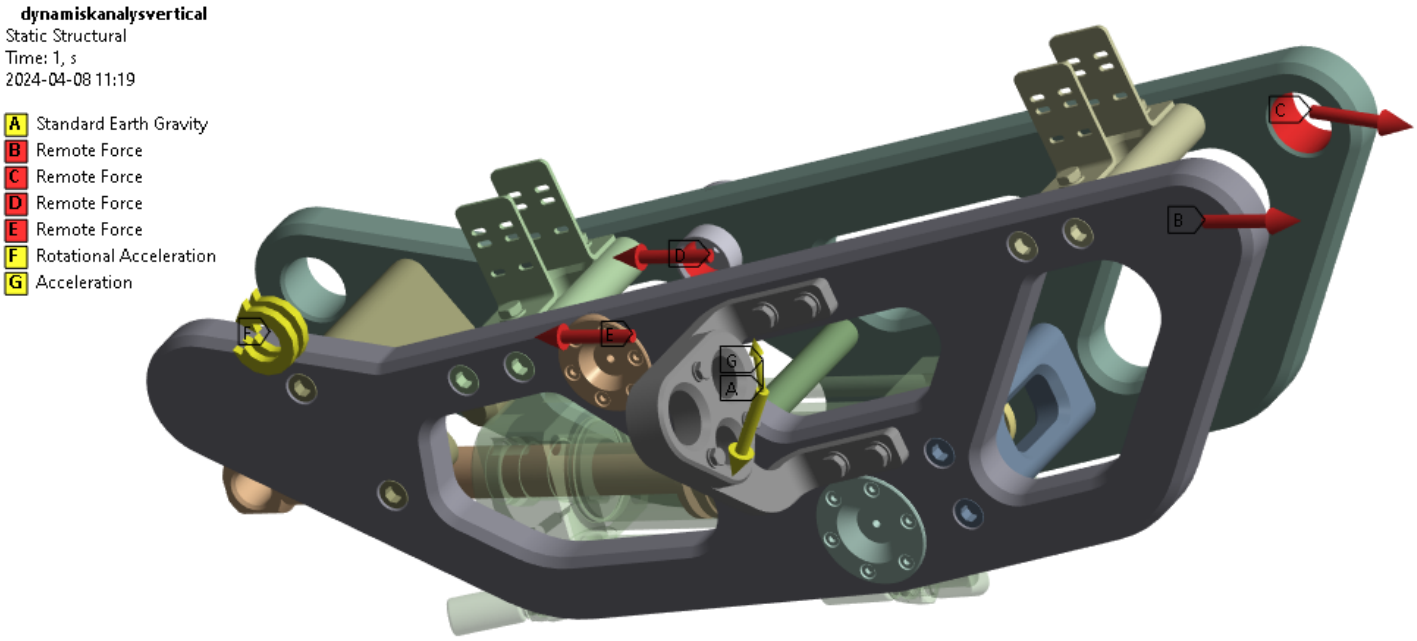

Figure 18: Force setup for section 3.

The mesh of section 3 can be found in Fig. 19. An element size of 9mm was chosen, as it was the smallest size feasible within the node/element limit of section 3, which happens to be the largest section. To maintain consistency, this same element size was applied across all sections. Additionally, steel components are treated as rigid.

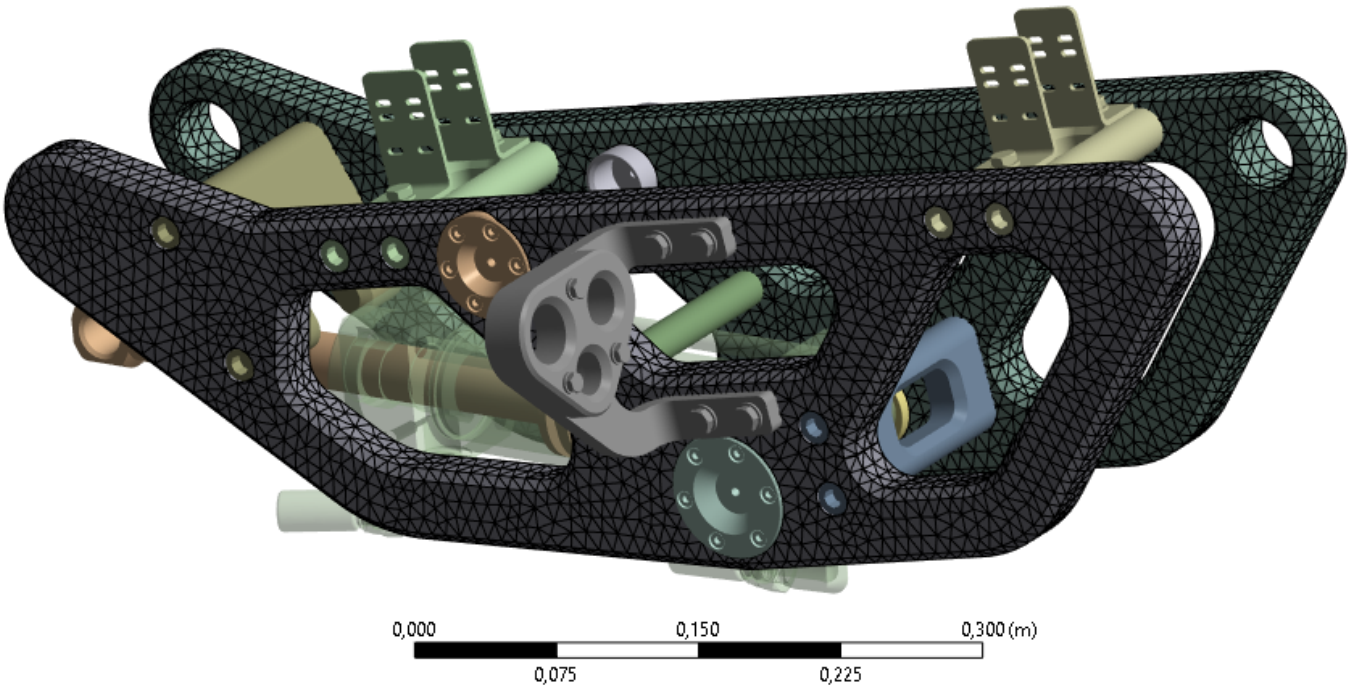

Figure 19: Mesh of section 3. It consists of 106 000 nodes and 61 000 elements.

3.2.2 FEM-analysis of Collision Scenarios

Initially, the idea was to use the same FEM-analysis procedure as described for the Rigid Dynamics load cases for the Collision Scenarios. However, it was not possible to extract the state of the system from the moment of impact to a Static Structural FEM analysis, which measurement of response forces indicated. The reason for this likely stemmed from transferring the rotational acceleration field into the FEM-analysis, as the rotational acceleration was highly localized within a section, and it was hard to find representative mean value of the entire section. Due to this, the FEM analysis of the collision scenarios were done directly in the collision simulation in Transient Structural. This meant that the entire manipulator had to be meshed under the node/element limit.

Initial simulation trials indicated that sections 1 and 2 were not of concern. The mesh quality of section 1 and 2 was decreased to leave room for increasing mesh quality of section 3-6. In sections 3 to 5, the element size was set to 1.2mm, while in section 6, it was set to 1mm. Section 6 received higher mesh quality because it comes into contact with the wall, and simulations converged more easily with higher mesh quality in this section. The mesh used in the collision scenarios is presented in Fig. 20. Once again, steel parts are set as rigid.

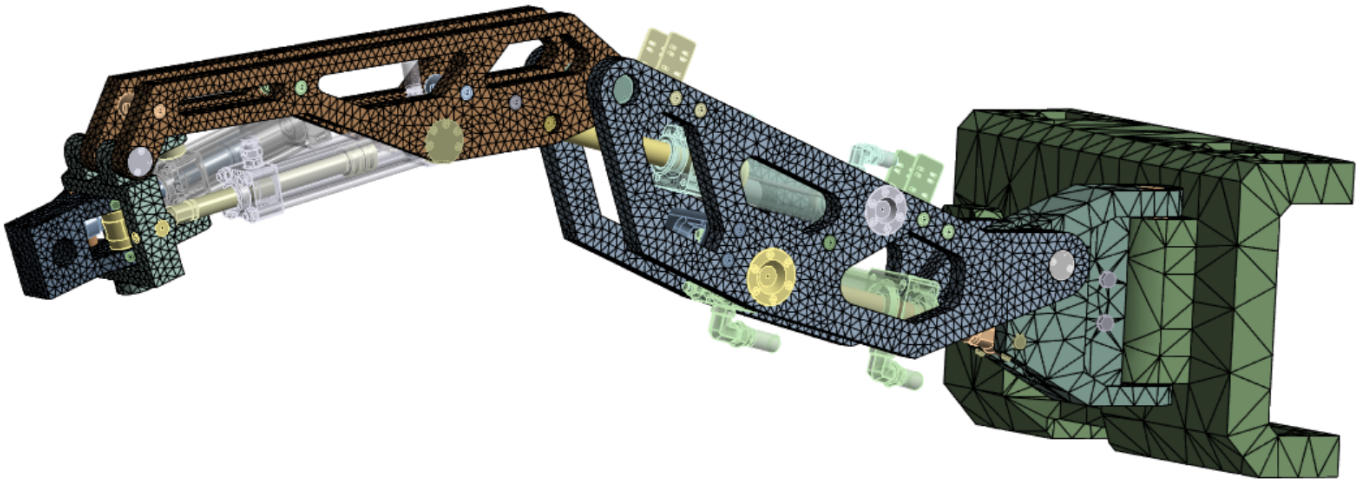

Figure 20: Collision Scenario mesh. It consists of 106 000 nodes and 61000 elements.

3.2.3 FEM analysis of steel parts

The FEM-analysis described so far is entirely focused on the big aluminium parts of the manipulator, where steel parts are treated as rigid. Steel parts that are deemed to be under high stress will also be analyzed through FEM-analysis. The steel parts analyzed are focused on those connecting sections and are defined in Fig. 21.

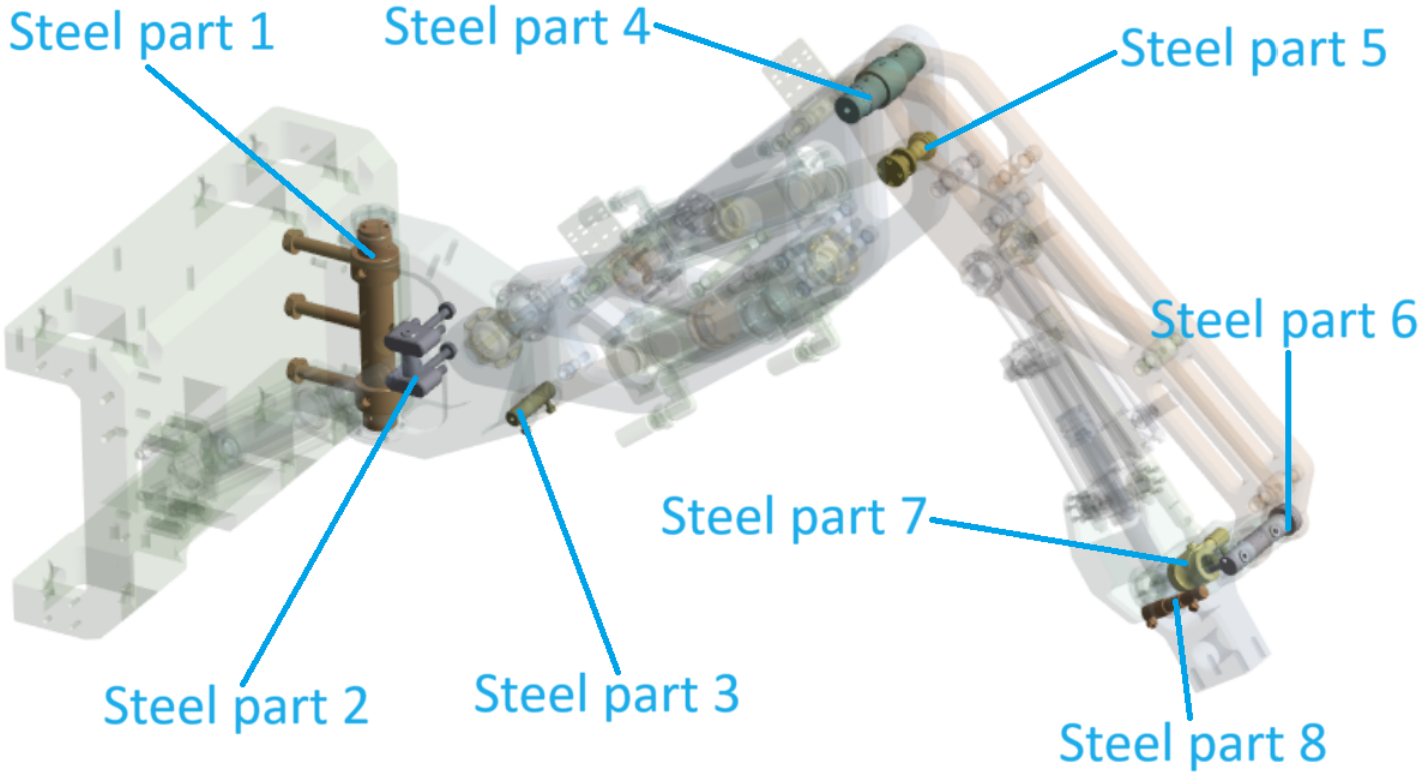

Figure 21: Steel parts that are analyzed.

The maximum load from the Rigid Dynamic load cases and collision scenarios will be used as boundary conditions. An initial analysis indicated that the steel parts used to connect the hydraulic cylinders on the piston side were the most vulnerable (Steel part 2, 3, 5, 7, 8). Due to this, the boundary conditions used to clamp these steel parts will be discussed in more detail. An example of how the boundary conditions are applied is demonstrated in Fig. 22. The boundary conditions are set up to firmly clamp regions A and B, while the load is applied as a remote force to region C.

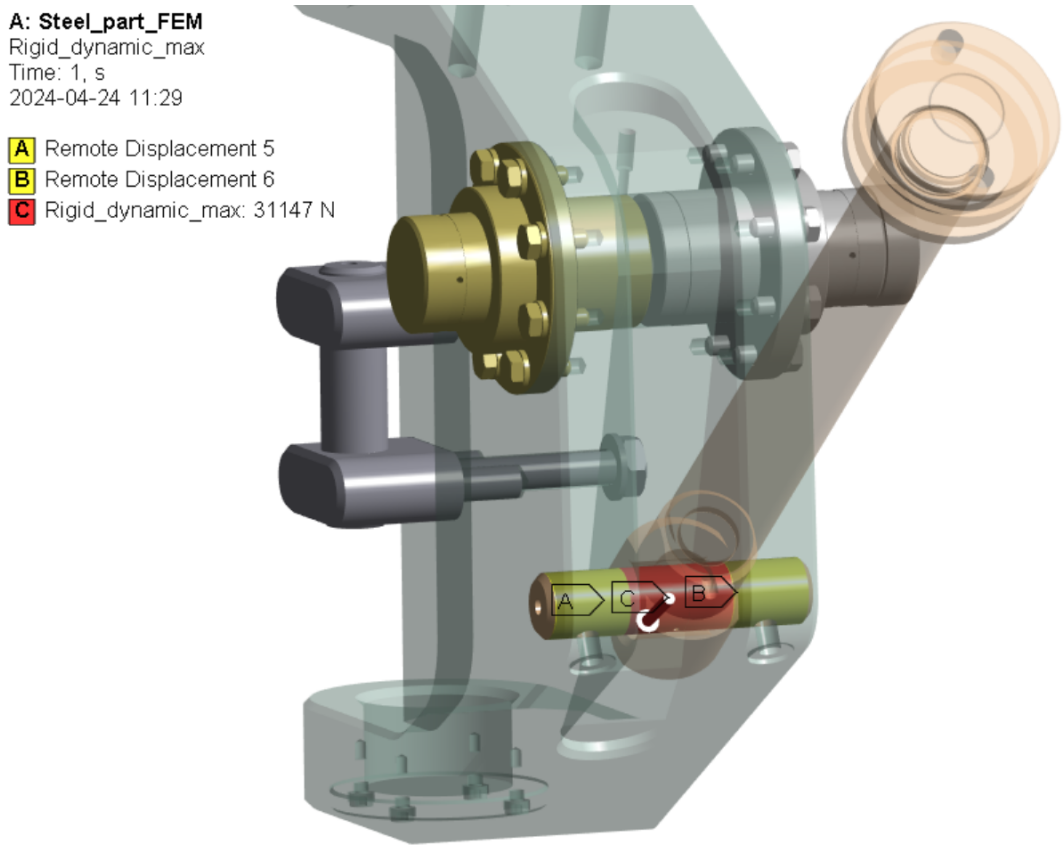

Figure 22: Example of how boundary conditions of steel part 2, 3, 5, 7 and 8 are applied.

3.3 Summary of load cases and FEM-analysis

A summary of load cases and corresponding FEM-analysis are provided in Table. 2.

Load Case	Load identification	FEM-analysis
Rigid Dynamics 1	Vertical lift, performed in Rigid Dynamics	FEM-analysed section by section in Static Structural. Steel parts treated as rigid.
Rigid Dynamics 2	Horizontal lift, performed in Rigid Dynamics	FEM-analysed section by section in Static Structural. Steel parts treated as rigid.
Collision scenario 1	Vertical Collision in outstretched position, in Transient Structural	FEM-analyses performed directly Transient Structural. Steel parts treated as rigid.
Collision scenario 2	Horizontal Collision in outstretched position, in Transient Structural	FEM-analyses performed directly Transient Structural. Steel parts treated as rigid.
Collision scenario 3	Horizontal Collision in curled up position, in Transient Structural	FEM-analyses performed directly Transient Structural. Steel parts treated as rigid.
Steel parts	Loads identified from previous load cases.	FEM-analyses on steel parts in Static Structural

Table 2: Summary of load cases and corresponding FEM-analyses.

With the load cases defined and how the FEM-analysis is performed in each case the next step is to evaluate the results to make conclusions about the structural integrity of the manipulator.

3.4 Results evaluation

To draw conclusions regarding the structural integrity of the manipulator, the aluminium and steel parts are treated separately. The Eurocode 9 is used for the aluminium parts, and Eurocode 3 is used for the steel parts. These standards provide guidelines on the safe design of aluminium and steel structures.

3.4.1 Aluminium parts analysis

The Eurocode 9 [1, p. 33] states that an aluminium structure should be:

- Designed for corrosion.
- Designed for sufficient fatigue life.
- Designed for wearing.
- Designed for accidental actions.
- Inspected and maintained.

As this report focuses on structural integrity, the criteria regarding corrosion, and inspection will not be evaluated in detail. The criteria regarding wearing and accidental actions is hard to apply to the manipulator, due to difficulties finding areas prone to wearing, and the framework for accidental actions tailored to construction contexts. The fatigue life criterion will be the primary focus of the analysis.

Eurocode 9: Fatigue life of aluminium

The Eurocode 9: Design of aluminium structures – Part 1-3: Structures susceptible to fatigue [10, p. 38] describes the method for fatigue life identification of an aluminium detail accordingly:

1. Identify the largest principle stress history variation over a cycle at a detail of interest.

2. Count the loads over a cycle according to the reservoir method.

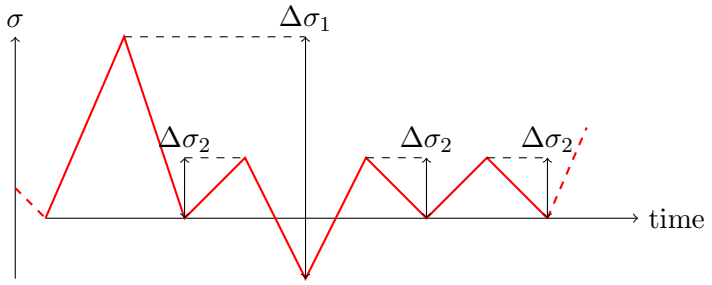

Figure 23: Reservoir method load counting over a cycle

3. Construct the stress range spectrum for a cycle.

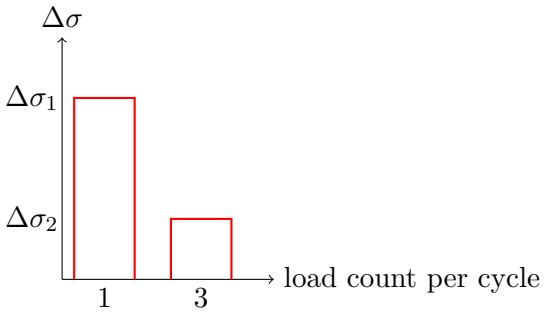

4. Decide fatigue life for each load. The fatigue life range of 10^3 to 10^5 loads to failure is described by:

$$N_i = (\frac{\Delta\sigma_c}{\Delta\sigma_i} \cdot \frac{1}{\gamma_{Ff}\gamma_{Mf}})^{m_0} \cdot 20^{\frac{m_0}{m_1}} \cdot 10^5 \tag{21}$$

The fatigue life range of 10^5 to $5 \cdot 10^6$ loads to failure is described by:

$$N_i = 2 \cdot 10^6 (\frac{\Delta\sigma_c}{\Delta\sigma_i} \cdot \frac{1}{\gamma_{Ff}\gamma_{Mf}})^{m_1} \tag{22}$$

The fatigue life range of $5 \cdot 10^6$ to 10^8 loads to failure is described by:

$$N_i = 5 \cdot 10^6 (\frac{\Delta\sigma_c}{\Delta\sigma_i} \cdot \frac{1}{\gamma_{Ff}\gamma_{Mf}})^{m_2} \cdot (\frac{2}{5})^{\frac{m_2}{m_1}} \tag{23}$$

Following the Eurocode 9, the aluminium parts are assumed to fall into the category of "sheets, plates, simple extruded rods, bars and machined parts with the stress parallel to the rolling direction, edges free of stress raisers and surface roughness of under $r_{z5} < 40\mu m$", which sets:

$\Delta\sigma_c = 90\text{MPa}$ and $m_1 = 7$.

The consequence class is set to the lowest, with the definition "small risk of fatal incident and small economic consequence in case of collapse", which sets:

$\gamma_{Mf} = 1$

The variable γ_{Ff} depends on a normal distribution of load intensities and if the construction can easily be inspected for crack initiation. As the manipulator can easily be inspected, and as the loads identified assumes "worst case" this parameter is set to

$\gamma_{Ff} = 1$

m_0 depends on R value, for values $R \geq 0$ m_1 is used. For $R = -1$, m_0 is equal to 4. For R values between 0 and -1 the m_0 is linearly interpolated.

Note 1: The models assume high tensile mean stress. If the mean stress is compressive or low tensile stress, the fatigue life may be increased.
Note 2: Loads with stress range below $\Delta\sigma_L$, assumed to be 10^8 loads according to Eurocode 9, are considered not to cause any damage. Utilizing Eq. 23 this yields a stress range of 56 MPa.

5. Decide number of cycles to fatige using the Palmgren-Miner rule.

$$\sum_{i=1}^{n} \frac{n_i}{N_i} \leq 1 \tag{24}$$

Applying the Palmgren-Miner rule to the example yields the number of cycles to fatigue n accordingly:

$$\frac{n}{N_1} + \frac{3n}{N_2} = 1 \tag{25}$$

3.4.2 Steel parts analysis

The Eurocode 3 is similar to the Eurocode 9 in its design. The criteria regarding corrosion, fatigue life, wear, accidental actions and maintenance are the same as presented in the Eurocode 3. Following the manner of the aluminium parts analysis, fatigue life is the primary focus of the steel part analysis.

Eurocode 3: Fatigue life of steel
Step 1-3 and step 5 are identical to the Aluminium fatigue life identification. However, in step 4, where the fatigue life of a load is calculated, there are some differences. The Eurocode 3 presents a simpler method of calculating fatigue life with the following relationships. [11, p. 15-16]

$$N_i \cdot \Delta\sigma_i^m = \Delta\sigma_c^m \cdot 2 \cdot 10^6 \qquad \text{with m=3, for fatigue life } N_i < 5 \cdot 10^6 \tag{26}$$

$$N_i \cdot \Delta\sigma_i^m = \Delta\sigma_c^m \cdot 5 \cdot 10^6 \qquad \text{with m=5, for fatigue life } 5 \cdot 10^6 < N_i < 10^8 \tag{27}$$

Where $\Delta\sigma_c$ just as with aluminium depends on detail category.

3.4.3 Applying the Eurocodes to the manipulator

With the fatigue life method of the Eurocodes presented, this section will explain how it is going to be applied to the FEM-results.

1. If a detail is close to its $R_{p0.2}$ stress, no fatigue life will be decided for the specific detail and load case.

2. The Rigid Dynamic FEM-analyses assesses stresses at a specific instant, which is the moment of peak load between sections in the Rigid Dynamic analyses. Consequently, determining a stress range solely from the Rigid Dynamic FEM-results is not possible, as it requires knowledge of the greatest variation in principal stress history. The stress range can however be approximated, with the following method: since the FEM-results display stresses at the moment of maximum load, it is assumed that the stress corresponds to a peak, visualised by point 1 in Fig. 24. After the manipulator is unloaded and standing still, stresses are assumed to be at their lowest point, corresponding to point 2 in Fig. 24. Due to this, the forces between sections is recorded when the manipulator is unloaded and at rest, and this is used to find the minimum principal stress. This allows for a construction of a stress range, offering a rough estimation of fatigue life for the Rigid Dynamic load cases.

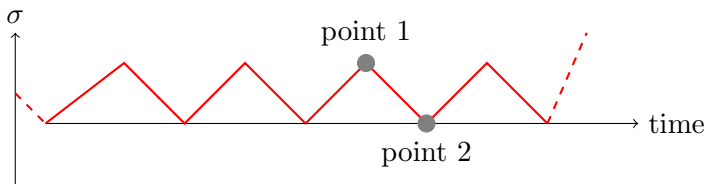

Figure 24: Example of load history

3. The Collision Scenarios are performed over several time steps, allowing for a stress range history construction. Determining this range involves identifying the maximum

and minimum principal stress over the simulation in a specific point of the manipulator. The difference in these being the stress range.

An aspect worth considering is that the Ansys modules lack an effective method for determining the effective stress range in a specific direction. For example, while the program can identify the maximum principal stress and its directional vector throughout the body, it does not include the feature to identify the minimum stress in the same direction throughout the simulation. As a result, the difference in value between the maximum principal stress at the moment of maximum load and the minimum principal stress when the manipulator is unloaded will be used to determine the stress range. Checks were performed to assess the parallelism of these stresses, and they indicated that the maximum and minimum principal stresses were not necessarily parallel, which is highlighted by the example check presented in the Appendix, chapter 7.1. However, due to absolute value of the minimum principal stress in all load cases being much lower than the maximum principal stress, this will likely not affect the accuracy of the stress range greatly. Additionally, the actual stress parallel to the maximum principal stress cannot be lower than the minimum principal stress, making the stress range slightly larger than the real stress range, making this method conservative.

3.5 Parts of the manipulator not analysed

There are certain parts of the manipulator where the structural integrity is not analysed, which is important to mention. Parts not analysed are:

- Steel parts not mentioned in Fig. 21.
- Individual bolts.
- Bronze bushings.
- Hydraulic cylinders.
- Linear Unit.

3.6 Extraction of stresses from FEM-analysis

When performing the the check for plasticity and retrieving stress ranges for fatigue life analysis, it is crucial to get representative values of the stresses. When using a linear elastic material model, stresses can exceed the real life stresses, particularly in sharp corners or close to stress raisers, such as small radii. For these reasons, stresses to be used in calculations or plasticity checks are not retrieved close to corners or stress raisers.

4 Results

The results chapter will present the FEM-analysis of each load case, together with an evaluation according to the procedure presented in chapter 3.4.3. The results are presented in three parts, with the Rigid Dynamics results presented firstly, Collision Scenarios presented secondly and small steel parts presented thirdly. Results presented will be focused on sections or parts under high load.

4.1 Rigid Dynamic stresses results

The Von-Mises effective stresses were well below the $R_{p0.2}$ for the vertical lifts across the entire manipulator. As plasticity is not of concern, the fatigue life will be analysed for the Rigid Dynamic load cases. Details that are identified to have the highest stresses are used for this analysis.

4.1.1 Vertical lift results

For the vertical lifts, one detail in Section 4, marked by a red square in Fig. 25 is identified as the point of highest stress range. The stress range for this specific detail is found according to the method described in chapter 3.4.3. In Fig. 25 the maximum principal stress in the moment of maximum load is displayed on the top, while the minimum principal stress, in the manipulators unloaded state is displayed on the bottom. The maximum principal stress is identified as 31 MPa, and the minimum is identified as -1 MPa, constructing a stress range of 32 MPa, well below the infinite fatigue life stress range $\Delta\sigma_L$ of 56 MPa.

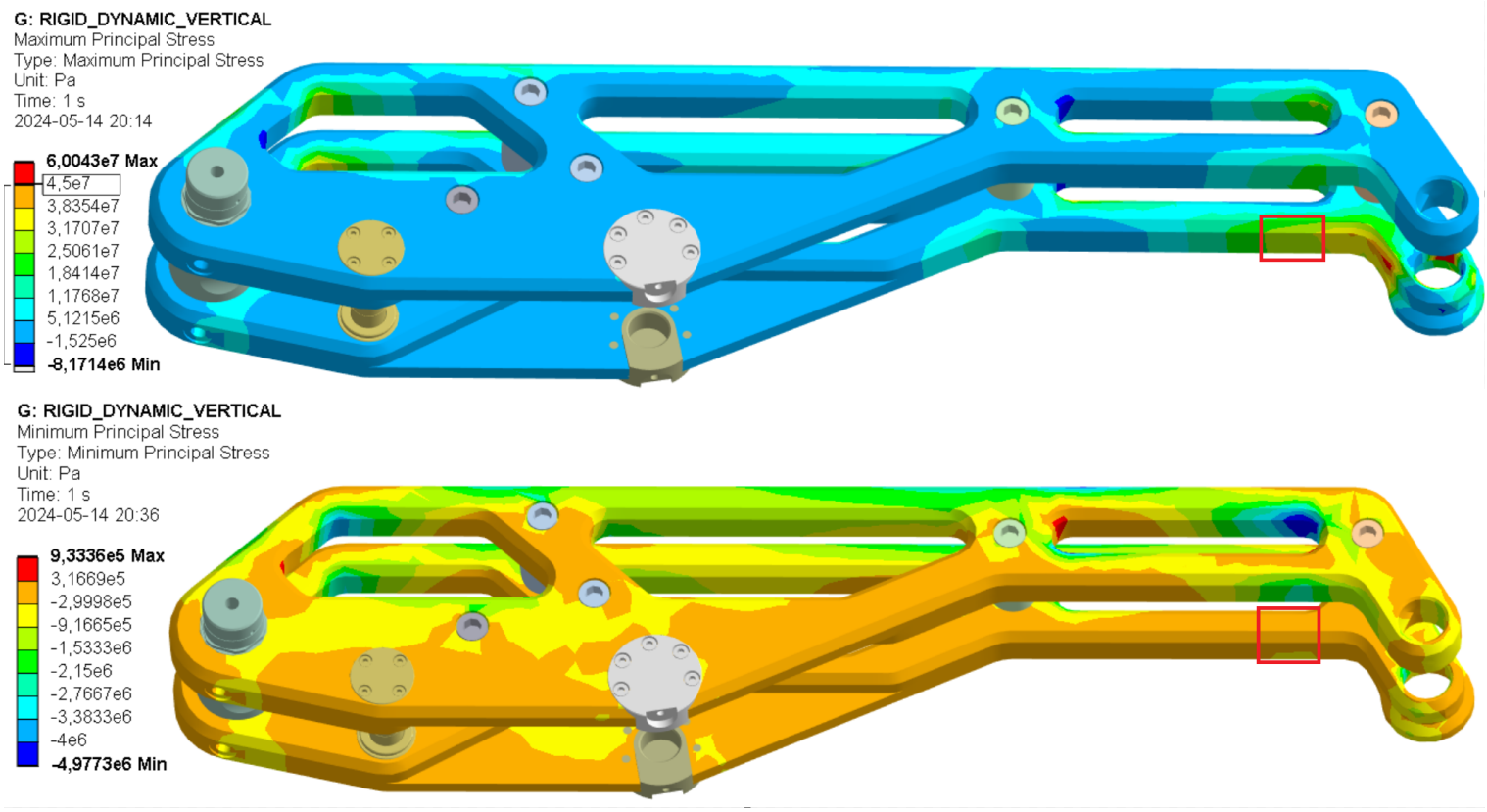

Figure 25: Maximum (top) and minimum (bottom) principal stress in section 4 for vertical lift. Red box indicates detail of analysis.

4.1.2 Horizontal lift results

For the horizontal lifts, the detail of highest stress range is marked by a red square in Fig. 26. The maximum principal stress is identified as 60 MPa, and the minimum is identified as 0 MPa, constructing a stress range of 60 MPa. According to Eq. 23, this stress range corresponds to a fatigue life of $5.9{\cdot}10^7$ cycles.

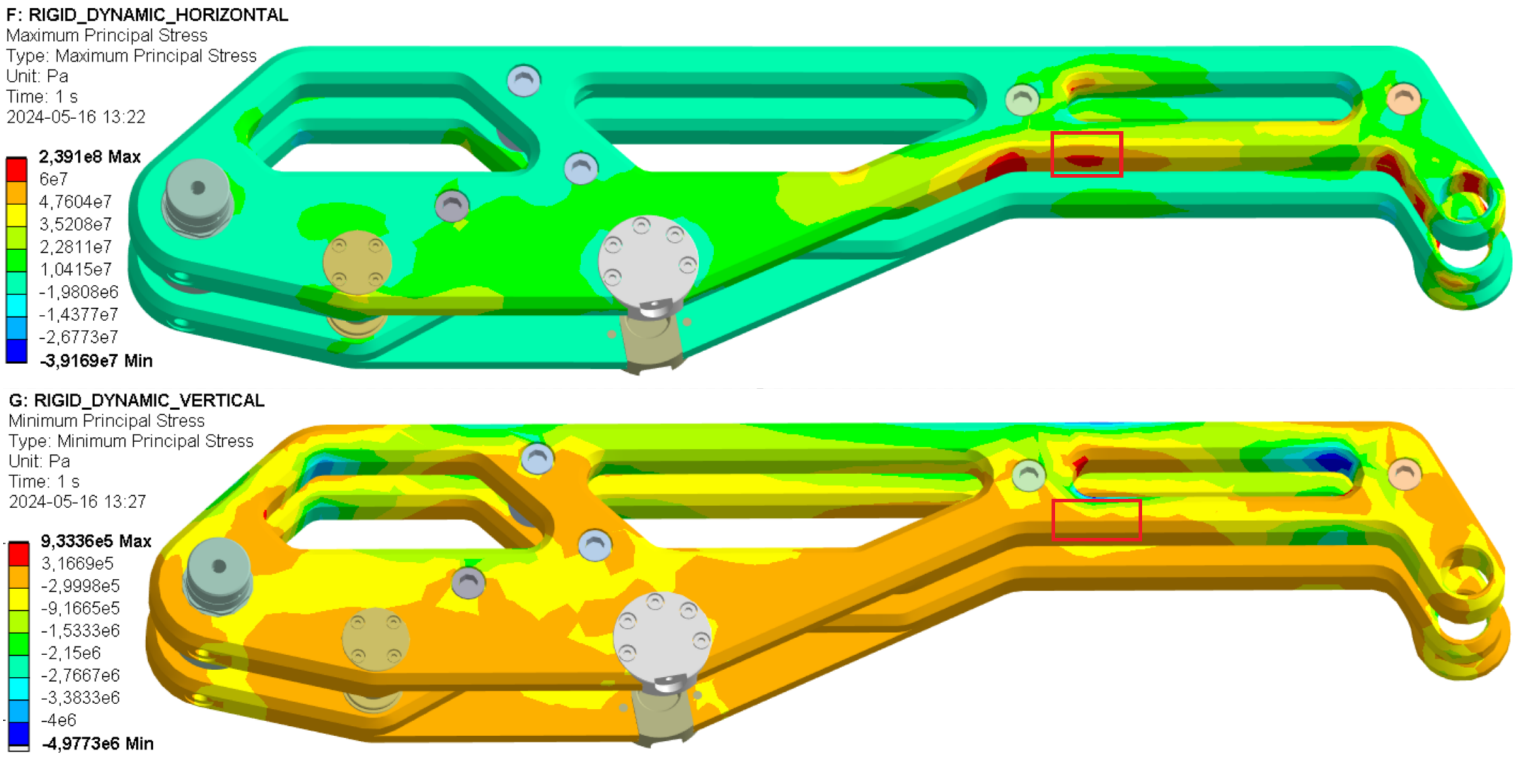

Figure 26: Maximum (top) and minimum (bottom) principal stress in section 4 for vertical lift. Red box indicates detail of interest.

4.1.3 Rigid Dynamic summary

According to FEM-analysis of the Rigid Dynamic load cases, the structural integrity of the aluminum parts is sufficient for lifts of the target weight of 150 kg. Neither plasticity nor fatigue life poses a threat to the aluminum parts.

4.2 Collision Scenarios stresses results

Stresses across the manipulator were significantly higher in the collision scenarios compared to the Rigid Dynamic load cases. The Von Mises effective stresses will be presented to indicate the safety margin concerning plasticity. Stresses exceeding the $R_{p0.2}$ of 250 MPa are marked in red. Additionally, areas identified to have a large stress range will be evaluated for fatigue life. Figures of principal stresses used to decide fatigue life are not presented in the results section, however one example is provided in the Appendix, chapter 7.2.

4.2.1 Collision Scenario 1

The Von-Mises effective stresses in the manipulator of Collision Scenario 1 are presented in Fig. 27. The highest Von-Mises effective stresses are about half of the $R_{p0.2}$. Analysis of principal stresses reveal two details to contain large stress ranges, which are marked by red squares in Fig. 27. The stress range for these details are found according to the method described in chapter 3.4.3, with the stress

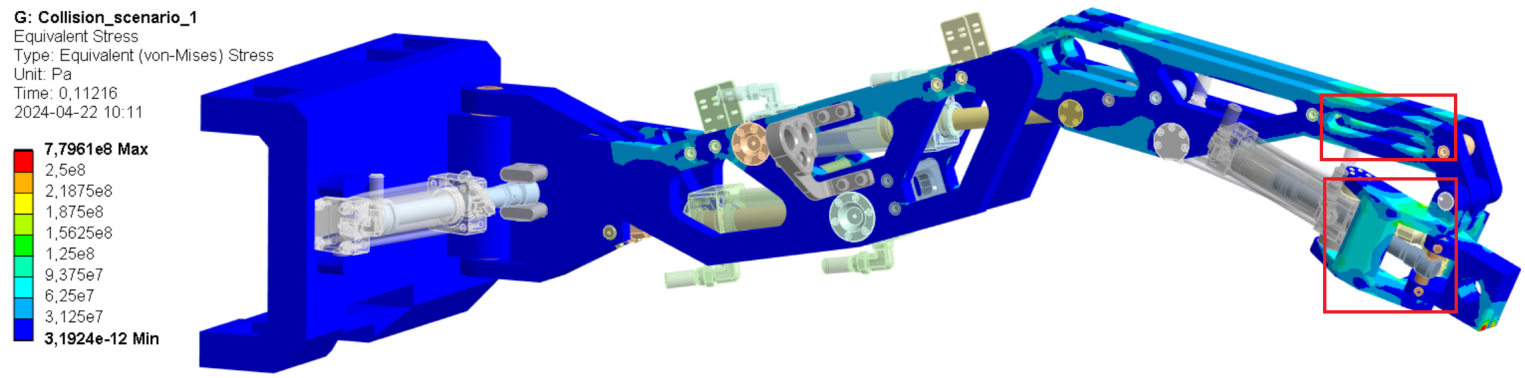

Figure 27: Von-Mises effective stress across the manipulator for Collision Scenario 2

4.2.2 Collision Scenario 2

The Von-Mises stresses in the manipulator of collision scenario 2 are presented in Fig. 28. Analysis of principal stresses reveal two details of the manipulator to contain large stress ranges, which are marked by red squares in Fig. 28. These areas are analysed for fatigue life.

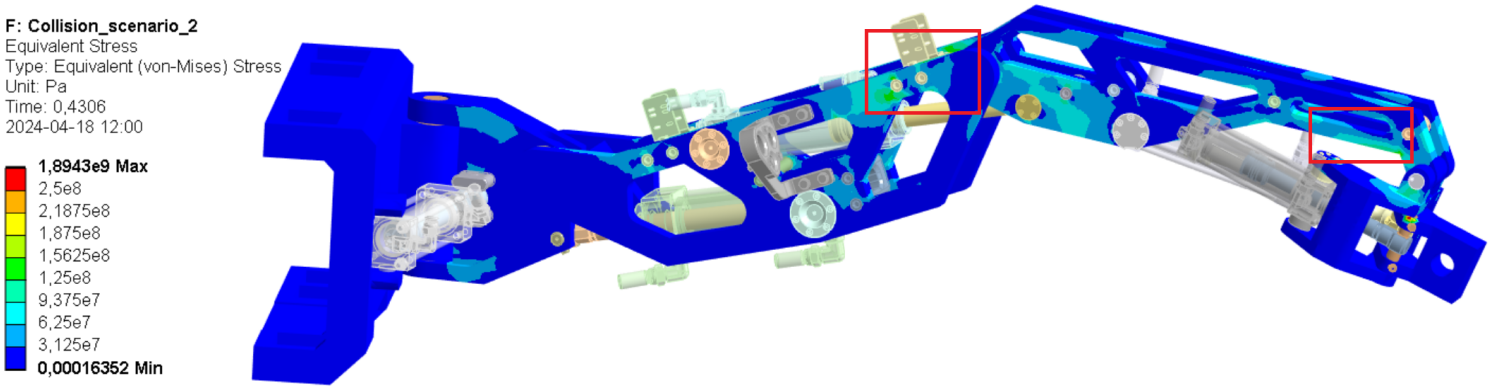

Figure 28: Von-Mises effective stress across the manipulator for Collision Scenario 2

4.2.3 Collision Scenario 3

The Von-Mises stresses in the manipulator of collision scenario 2 are presented in Fig. 29. Analysis of principal stresses reveal two details of the manipulator to contain large stress ranges, which are marked by red squares in Fig. 29. These areas are analysed for fatigue life.

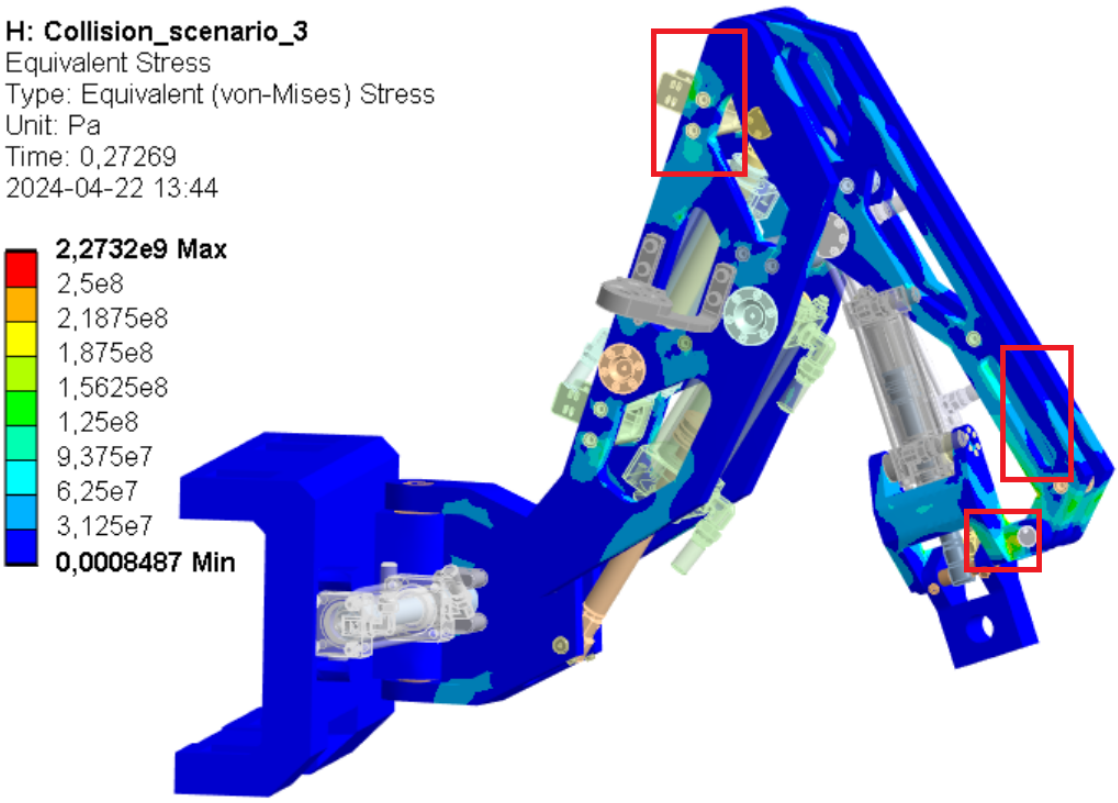

Figure 29: Von-Mises effective stress across the manipulator for Collision Scenario 3

4.2.4 Collision Scenarios summary

The loads to failure of the different collision scenarios and sections are presented in Table. 3.

Load case	**Collision Scenario 1**	**Collision Scenario 2**	**Collision Scenario 3**
Section 1	-	-	-
Section 2	-	-	-
Section 3	-	595000	55000
Section 4	55000	956000	300000
Section 5	55000	-	160000

Table 3: Loads to failure N for each section and Collision Scenario

According to the analysis of the Collision Scenarios, plasticity is not of concern for the aluminium parts for collision scenarios. The estimated fatigue life is about 55000 loads to failure.

4.3 Steel parts

In general, the steel parts contain sizable regions close or above its plastic stress. Due to this, no fatigue life will be decided. Instead, the Von-Mises effective stresses in comparison to the $R_{p0.2}$ of the steel alloy is used to get an understanding of the structural integrity of the steel parts. Steel part 1, 4 and 6 are presented in the appendix. Steel part 2, 3, 5, 7 and 8 are similar in their design and function, and the results are similar. For this reason steel part 3 (which is under the highest load) is used to represent the results of these steel parts.

4.3.1 Steel part 3

The Von-mises stresses of steel part 3 are presented in Fig. 30. For the Collision Scenarios there are sizable regions above the $R_{p0.2}$. The stresses in the Rigid Dynamic load case are somewhat below the $R_{p0.2}$.

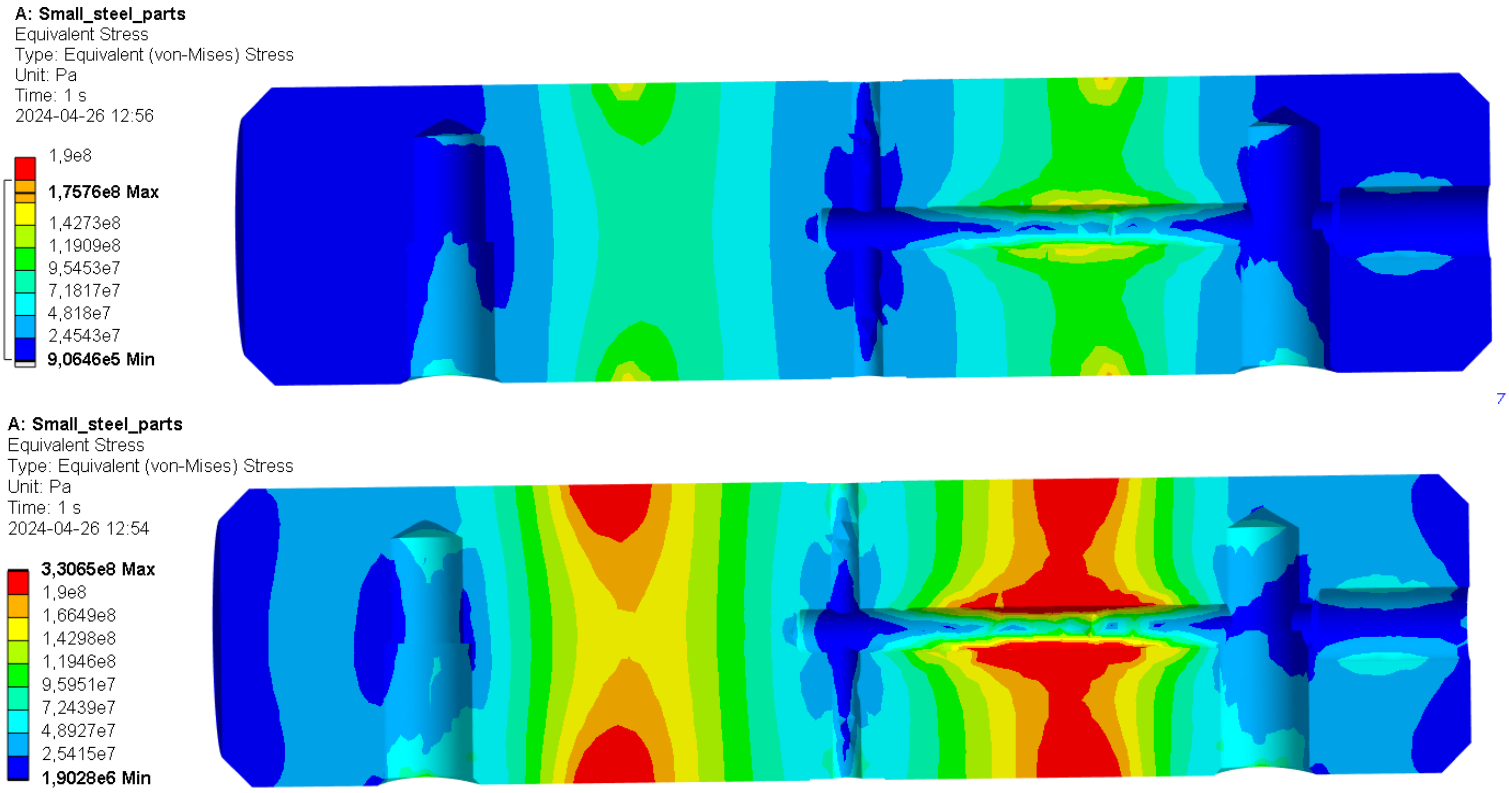

Figure 30: Von-Mises stress in cross section of steel part 3 for maximum load in Rigid Dynamic load case (top) and Collision Scenario max load (bottom). The cross section parallel to the axle of the steel part is displayed in the figure.

4.3.2 Summary steel parts

A summary of the risk of plasticity analysis for all steel parts is presented in Table. 4.

Load case	**Rigid Dynamic max load**	**Collision Scenario max load**
Steel part 1	Well below $R_{p0.2}$	Small regions above $R_{p0.2}$
Steel part 4	Well below $R_{p0.2}$	Small regions above $R_{p0.2}$
Steel part 6	Well below $R_{p0.2}$	Small regions above $R_{p0.2}$
Steel part 2	Below $R_{p0.2}$	Sizable regions above $R_{p0.2}$
Steel part 3	Below $R_{p0.2}$	Sizable regions above $R_{p0.2}$
Steel part 5	Below $R_{p0.2}$	Sizable regions above $R_{p0.2}$
Steel part 7	Below $R_{p0.2}$	Sizable regions above $R_{p0.2}$
Steel part 8	Below $R_{p0.2}$	Sizable regions above $R_{p0.2}$

Table 4: Summary of comparison of Von-Mises effective stresses and the $R_{p0.2}$ for the steel parts and load cases.

5 Discussion

5.1 Discussion of results

The results indicate that the aluminum parts are well designed for lifting the target weight of 150 kg and can handle collisions. The fatigue life is not of concern as the calculated fatigue life of 55 000 cycles is more than sufficient. Additionally, these fatigue calculations assume that each collision occurs in exactly the same manner, whereas in reality, variations in impact speed, angle, and direction will occur. Taking this into account, the structural integrity of the aluminium parts is adequate.

The results for the steel parts are different. The comparison of stresses retrieved and the $R_{p0.2}$ shows that the steel parts are at risk of undergoing plastic deformation, especially when subjected to the boundary conditions of the collision scenarios. Even with the Rigid Dynamic loads, the safety margin is not particularly large. The steel parts connected to the piston side of the cylinders are especially vulnerable.

Given the results, the fatigue life calculations for the aluminum parts did not necessitate the use of load counting or the application of the Palmgren-Miner rule as described in the Eurocode. Additionally, the fatigue life calculations for the steel parts were not conducted since these components were found to be at risk of plastic deformation.

5.2 Improvements

The first and perhaps most crucial step is to address the steel parts at risk of undergoing plasticity. The simplest solution is to use a different steel alloy for these parts, avoiding the need to alter any geometries. It is important to choose an alloy with great corrosion resistance due to the humid environment in which the manipulator operates. Due to this, a high strength stainless steel alloy would be a great choice of material for the steel parts. While steel part 2, 3, 5, 7 and 8 are the most vulnerable, and require change of material the most urgent, it might also be beneficial to also change the steel used in part 1, 4 and 6, as these steel parts too do not show great margin of safety to plasticity. Before installing the new steel alloy, an analysis should be performed to confirm they are sufficiently robust to handle the loads.

Another useful improvement for the manipulator, especially if it is equipped with a gripper tool for lifting, would be to design a safety system that activates before a collision occurs. The current analysis does not account for collisions while the manipulator is loaded, and the stresses on the manipulator are likely to be even higher in such scenarios. Additionally, the component being handled can be damaged in the case of a collision. Therefore, it is preferable to avoid collisions altogether when the manipulator is loaded. This safety system could utilize detectors to identify fast-approaching walls or objects, triggering the safety system to slow down the manipulator.

5.3 Sources of error

Due to the the inability to retrieve input data from the real-life manipulator and the problem being complex, there are numerous uncertainties in the analysis.

The load identification process depends on analyzing videos of the manipulator and discussions with the Fagerström team to determine its motion pattern. Consequently, the velocity and acceleration data used in the Rigid Dynamic cases and collision Scenarios are not derived from actual measurements of the real-life manipulator. This introduces uncertainty into subsequent analyses, affecting the loads applied and the stresses obtained from the FEM-analysis.

The Collision Scenarios will be further discussed, particularly the conservative approach to set them up. The significance of exploring the collision scenarios stem from the fact that the manipulators safety systems do not activate during collisions, causing the cylinders to remain engaged throughout the collision. Initially, an attempt was made to gradually increase the pressure (which translates to the force exerted by the cylinder) to the maximum as the manipulator made contact with the wall. However, this method failed because the manipulator bounced off the wall before any significant pressure could build up. Therefore, the pressure was set to the maximum in the cylinder before impact, which would not occur in the real-life manipulator. Additionally, all other cylinders are modeled as completely stiff (except for the inherent stiffness of the steel material itself), whereas in reality, the flow ports of these cylinders might be slightly open to allow for damping. Moreover, the aluminum material itself has some damping properties, represented by the term $\boldsymbol{C}\dot{\boldsymbol{u}}$ in Eq. 18. This term was not used, which means that some excessive vibrations might have influenced the results. Additionally, the wall is modeled to be completely rigid and fixed in space, which probably is not the case in reality.

Another source of error worth mentioning is that in the Collision Scenarios and in the analysis of the Rigid Dynamics horizontal lift, only one direction of the swing is analyzed. Consequently, one side of the arm experiences compression while the other experiences tension. In reality, however, the manipulator collides and swings in both directions, subjecting one detail of the manipulator to both compression and tension, increasing the stress range of a single detail. A simulation of the manipulator colliding and swinging in both directions could have been used to find this combined stress range, but was not used due to time restriction. This error will affect the stress range retrieved for the fatigue life analysis.

Additionally, it is worth mentioning that no mesh convergence study was done due to time restrictions, and for the Rigid Dynamic load case, the manipulator is modelled as rigid, while in reality, the flexibility of the material might have influenced the results.

6 Conclusion

In conclusion, the results of the manipulator are mixed. While the aluminium sections are sufficiently robust for handling the target weight and can withstand collisions, the steel parts are at risk of undergoing plastic deformation, especially in collision scenarios. Reinforcing the steel parts will allow Fagerström to proceed with outfitting the manipulator with a gripper tool.

References

[1] *Eurocode 9: Design of aluminium structures – Part 1-1: General structural rules*. SIS Svenska Institutet för Standarder, 2007.

[2] *Eurocode 3 – Design of steel structures – Part 1-1: General rules and rules for buildings*. SIS Svenska Institutet för Standarder, 2022.

[3] *Mechanical User's Guide*. URL: https://ansyshelp.ansys.com/account/secured?returnurl=/Views/Secured/corp/v241/en/wb_sim/ds_Home.html.

[4] *Eurocode 3: Design of steel structures – Part 1-4: General rules – Supplementary rules for stainless steels*. SIS Svenska Institutet för Standarder, 2006.

[5] A.P. Jivkov K. Berbatov B.S. Lazarov. "A guide to the finite and virtual element methods for elasticity". In: *Applied Numerical Mathematics* 169 (2021), pp. 351–395.

[6] N. Petersson Saabaye Ottosen. *Introduction to the FINITE ELEMENT METHOD*. Pearson Education Limited, 1992.

[7] H.P. Lee J.S. Sun K.H. Lee. "Comparison of implicit and explicit finite element methods for dynamic problems". In: *Journal of Materials Processing Technology* 105.1–2 (2000), pp. 110–118.

[8] *Ansys Innovation courses: Implicit and Explicit Time Integration Methods — Lesson 2*. URL: https://courses.ansys.com/index.php/courses/time_integration/lessons/implicit-and-explicit-time-integration-methods-lesson-2/.

[9] François Faure Jérémie Allard Hadrien Courtecuisse. "Chapter 21 - Implicit FEM Solver on GPU for Interactive Deformation Simulation". In: *GPU Computing Gems Jade Edition* 169 (2012), pp. 281–294.

[10] *Eurocode 9: Design of aluminium structures – Part 1-3: Structures susceptible to fatigue*. SIS Svenska Institutet för Standarder, 2007.

[11] *Eurocode 3: Design of steel structures – Part 1-9: Fatigue*. SIS Svenska Institutet för Standarder, 2008.

7 Appendix

7.1 Check of collinearity between max/min principal stresses

Fig. 31 presents a check to see how parallel the maximum and minimum principal stress directions are for the vertical lifts results, presented by red squares in Fig. 25. The check reveals that maximum principal stress direction from moment of maximum load is not parallel to the minimum principal stress when unloaded, which also was the general case for other details being checked.

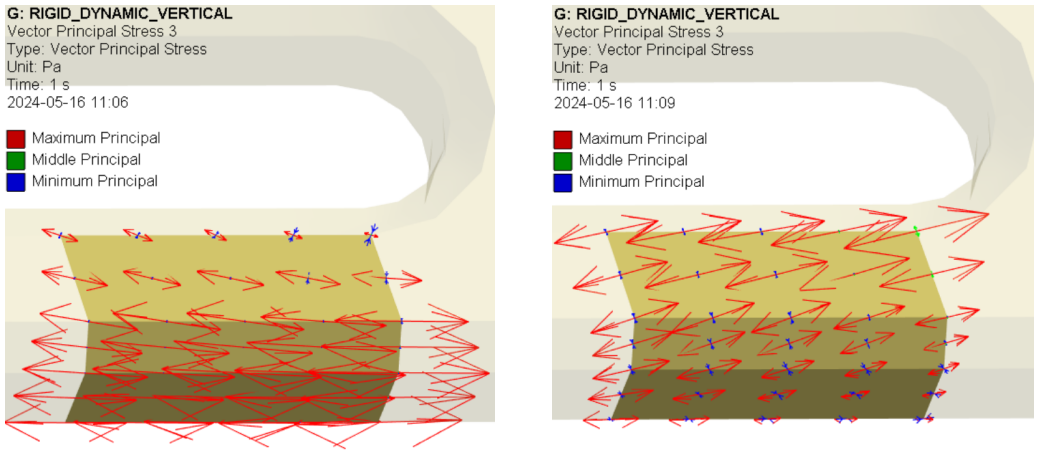

(a) Maximum load principal stress directions.

(b) Unloaded principal stress directions.

Figure 31: Comparison pf principal stress directions for the vertical lift.

7.2 Collision Scenario 1: Section 4 analysis

Maximum principal stresses of the identified vulnerable region in section 4 is demonstrated in Fig. 32. The maximum principal stress is approximated to be 150 MPa. The lowest principal stress in the same area is approximated to be 0, giving a stress range of 150 MPa.

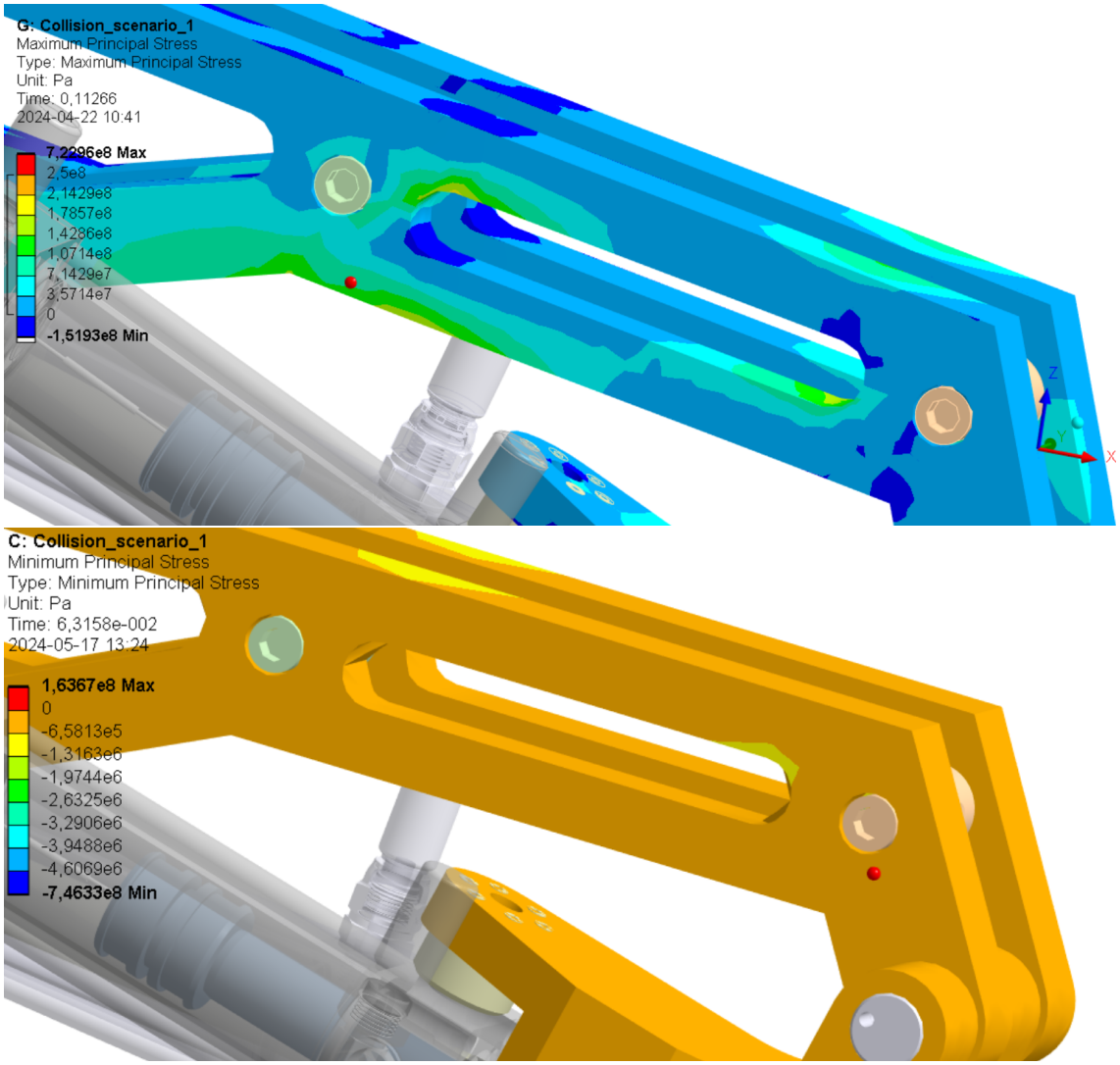

Figure 32: Maximum (top) and minimum (bottom) principal stress in section 4 for Collision Scenario 1.

7.2.1 Steel part 1, 4 and 6

The Von-mises stresses of steel part 1, 4 and 6 under max load from collision scenarios are presented in Fig. 33, Fig. 34 and Fig. 35. In each steel part, there are small regions with stress levels above the $R_{p0.2}$.

Steel part 1

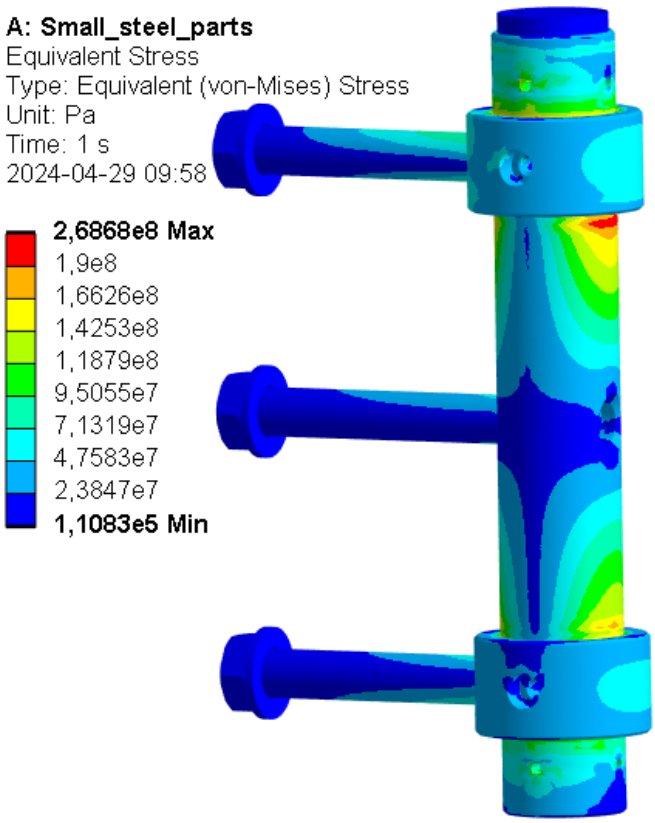

Figure 33: Von-Mises effective stress in steel part 1 loaded with collision scenario 1

Steel part 4

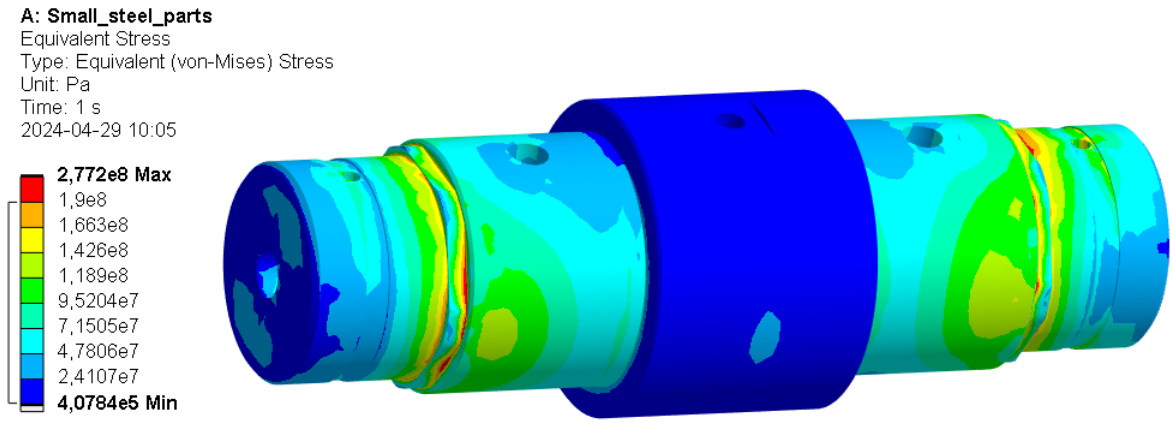

Figure 34: Von-Mises stress effective in steel part 4 for Collision Scenario 1.

Steel part 6

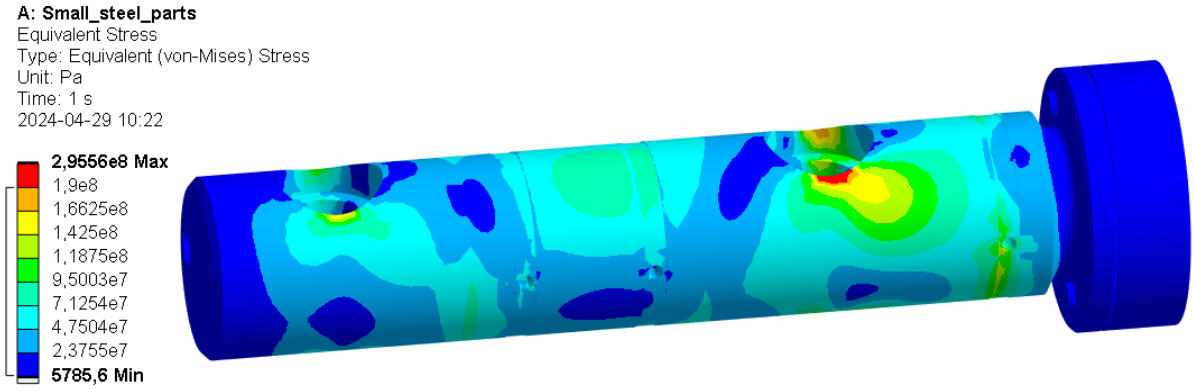

Figure 35: Von-Mises stress effective in steel part 6 for Collision Scenario 1.